

## Full Length Article

## Ballistocardiogram artifact correction taking into account physiological signal preservation in simultaneous EEG-fMRI



Rodolfo Abreu<sup>a,\*</sup>, Marco Leite<sup>a,b,c</sup>, João Jorge<sup>a,d</sup>, Frédéric Grouiller<sup>e</sup>, Wietske van der Zwaag<sup>f</sup>, Alberto Leal<sup>g</sup>, Patrícia Figueiredo<sup>a</sup>

<sup>a</sup> Institute for Systems and Robotics and Department of Bioengineering, Instituto Superior Técnico, Universidade de Lisboa, Lisbon, Portugal

<sup>b</sup> Department of Clinical and Experimental Epilepsy, University College London Institute of Neurology, Queen Square, London, WC1N 3BG, UK

<sup>c</sup> The Wellcome Trust Centre for Neuroimaging, University College London Institute of Neurology, Queen Square, London, WC1N 3BG, UK

<sup>d</sup> Laboratory for Functional and Metabolic Imaging, École Polytechnique Fédérale de Lausanne, Lausanne, Switzerland

<sup>e</sup> Biomedical Imaging Research Center (CIBM), Department of Radiology and Medical Informatics, Geneva, University Hospital, University of Geneva, Geneva, Switzerland

<sup>f</sup> Biomedical Imaging Research Center (CIBM), École Polytechnique Fédérale de Lausanne, Lausanne, Switzerland

<sup>g</sup> Centro de Investigação e Intervenção Social and Department of Neurophysiology, Centro Hospitalar Psiquiátrico de Lisboa, Lisbon, Portugal

## ARTICLE INFO

## Article history:

Received 16 October 2015

Accepted 14 March 2016

Available online 22 March 2016

## Keywords:

Ballistocardiogram

Electroencephalography

fMRI

Independent Component Analysis

## ABSTRACT

The ballistocardiogram (BCG) artifact is currently one of the most challenging in the EEG acquired concurrently with fMRI, with correction invariably yielding residual artifacts and/or deterioration of the physiological signals of interest. In this paper, we propose a family of methods whereby the EEG is decomposed using Independent Component Analysis (ICA) and a novel approach for the selection of BCG-related independent components (ICs) is used (PROjection onto Independent Components, PROJIC). Three ICA-based strategies for BCG artifact correction are then explored: 1) BCG-related ICs are removed from the back-reconstruction of the EEG (PROJIC); and 2–3) BCG-related ICs are corrected for the artifact occurrences using an Optimal Basis Set (OBS) or Average Artifact Subtraction (AAS) framework, before back-projecting all ICs onto EEG space (PROJIC-OBS and PROJIC-AAS, respectively). A novel evaluation pipeline is also proposed to assess the methods performance, which takes into account not only artifact but also physiological signal removal, allowing for a flexible weighting of the importance given to physiological signal preservation. This evaluation is used for the group-level parameter optimization of each algorithm on simultaneous EEG-fMRI data acquired using two different setups at 3 T and 7 T. Comparison with state-of-the-art BCG correction methods showed that PROJIC-OBS and PROJIC-AAS outperformed the others when priority was given to artifact removal or physiological signal preservation, respectively, while both PROJIC-AAS and AAS were in general the best choices for intermediate trade-offs. The impact of the BCG correction on the quality of event-related potentials (ERPs) of interest was assessed in terms of the relative reduction of the standard error (SE) across trials: 26/66%, 32/62% and 18/61% were achieved by, respectively, PROJIC, PROJIC-OBS and PROJIC-AAS, for data collected at 3 T/7 T. Although more significant improvements were achieved at 7 T, the results were qualitatively comparable for both setups, which indicate the wide applicability of the proposed methodologies and recommendations.

© 2016 Elsevier Inc. All rights reserved.

## Introduction

The complementarity between the high temporal resolution of electroencephalography (EEG) and the millimeter spatial resolution of functional magnetic resonance imaging (fMRI) has strongly motivated the integration of these two neuroimaging techniques (for reviews, please refer to Jorge et al., 2013; Murta et al., 2015). Simultaneous EEG-fMRI acquisitions, however, induce two major artifacts on EEG data. Firstly, the rapidly-changing, high-amplitude MR-related artifacts are induced by the switching of magnetic fields during the fMRI

acquisition. The gradient-related artifact occurrences are practically time-invariant and the use of standard average artifact subtraction (AAS) methods usually yields acceptable artifact reduction (Allen et al., 2000).

The correction for the ballistocardiogram (BCG) artifact represents a bigger challenge, mainly due to its non-stationary nature. As discussed in (Mullinger et al., 2013; Yan et al., 2010), several mechanisms contribute to the BCG artifact, the most plausible being: 1) the rotation of the head inside a strong, static magnetic field due to the cardiac pulse (Bonmassar et al., 2002), 2) the Hall effect of the pulsatile blood flow, which is an electrically conductive fluid, inducing changes of the voltage measured on the surface of the scalp (Tenforde et al., 1983) and 3) voltages generated by movement associated with pulse-driven expansion

\* Corresponding author at: Av. Rovisco Pais, 1 1049-001 Lisboa, Portugal.  
E-mail address: [rodolfo.abreu@ist.utl.pt](mailto:rodolfo.abreu@ist.utl.pt) (R. Abreu).

of the scalp (Debener et al., 2008). Studies aiming at a better characterization of the contribution of each of those mechanisms to the BCG artifact have found that most of the artifact variance is explained by flow-induced Hall voltage and pulse-driven head rotation (Mullinger et al., 2013). Additionally, a significant increase of the amplitude of the BCG artifact with the static magnetic field strength,  $B_0$ , has also been shown (Debener et al., 2008; Neuner et al., 2013), with severely hampered visual inspection of typical EEG patterns at 7 T. The accurate removal of the BCG artifact while preserving the physiological EEG signal is of utmost importance in several applications, particularly when the quantification of EEG features allows the prediction of blood-oxygen-level dependent (BOLD)-fMRI signal changes (e.g., Rosa et al., 2010), including epilepsy applications (Leite et al., 2013).

The BCG artifact occurrences are known to be approximately time-locked with the cardiac cycle; therefore, an AAS algorithm can be employed whereby an artifact template is extracted by averaging across multiple cardiac cycles, and a time-domain subtraction is then performed for artifact correction (Allen et al., 1998). In the most common approach, a moving average template is computed from successive artifact occurrences, assuming that the BCG artifact occurrences change slowly over time. The BCG variability can be more accurately taken into account by computing the temporal Principal Component Analysis (tPCA) over all the time-locked occurrences of the artifact in order to build an optimal basis set (OBS), comprising a given number of principal components (PCs) that explain the BCG artifact variance to some extent (Niazy et al., 2005). This basis set is then fitted to, and subtracted from, each artifact occurrence. More direct approaches to correct for the BCG artifact have been proposed, which are based on the use of motion sensors (Bonmassar et al., 2002; Chowdhury et al., 2014; Jorge et al., 2015a; Masterton et al., 2007). However, currently these techniques require hardware-related changes of the experimental apparatus and may therefore not be applicable in general.

A third category of BCG artifact correction methods is based on blind source separation. Independent Component Analysis (ICA) is commonly used for this purpose. By removing the contribution of independent components (ICs) reflecting artifact-related processes in the back-reconstruction of the EEG signal, an artifact-corrected signal can be obtained (Béнар et al., 2003; Mantini et al., 2007; Srivastava et al., 2005). Most of the ICA algorithms, however, assume spatial stationarity of the sources, ignoring the spatio-temporal variability of the BCG artifact occurrences (Debener et al., 2008; Vanderperren et al., 2007). Many approaches nevertheless rely on ICA-based methods, since alternative methods present their own limitations as well (Vanderperren et al., 2010). When using ICA-based EEG de-noising methods, several questions arise regarding: 1) the implementation of the ICA decomposition of EEG data to be used; 2) the number of ICs to be estimated; and 3) the identification of the ICs to be classified as BCG-related. All three issues have been addressed in (Vanderperren et al., 2010); however, the objective and accurate classification of ICs remains a major concern and several criteria can be found in the literature for that purpose, which will be presented and discussed later in this paper.

Due to the relative advantages and disadvantages of OBS and ICA-based methods, the combination of both has already been proposed (Debener et al., 2005, 2007). The OBS method is used to remove most of the BCG artifact contribution, followed by an ICA decomposition of the OBS-corrected EEG data to further remove residual artifacts. Despite its effectiveness in removing the artifact, the application of OBS directly on the EEG signal may also induce undesirable physiological signal reductions, which would be exacerbated if an additional step of ICA-based correction is applied. Recently, it has also been proposed to use a modified version of OBS in the IC space instead (Liu et al., 2012). For that purpose, the EEG data is first decomposed into a set of ICs and the mutual information (MI) (Bell and Sejnowski, 1995) between them and the electrocardiography (ECG) data is computed. The number of ICs with the highest MI is then chosen by means of a modified method (Peng et al., 2005) that finds the optimal number of ICs yielding minimal

error in leave-one-out cross-validation. The BCG-related ICs are removed from the back-reconstruction of the EEG signal and all the remaining ICs are singular value decomposition (SVD)-corrected before back-projecting them onto the EEG space, as it is hypothesized that the BCG artifact contributes to all ICs to varying degrees due to its non-stationary nature (Liu et al., 2012).

Regardless of the BCG artifact correction method used, the quality of the correction should be assessed (Freyer et al., 2009; Grouiller et al., 2007). Typically, event-related simultaneous EEG-fMRI studies are conducted and the performance of a given method can be computed based on features extracted from the event-related potentials (ERPs) of interest, such as: the inter-trial variability (Vanderperren et al., 2010), the signal-to-noise (SNR) ratio (Debener et al., 2007) or the difference between the ERPs extracted from the inside-MR EEG datasets and those that are obtained from the BCG artifact-free outside-MR EEG data (Mantini et al., 2007). When the frequency content of a task-modulated EEG signal is known, the power of the EEG within that frequency band can also be computed before and after BCG artifact correction (Xia et al., 2014). In resting-state fMRI (rs-fMRI) studies, the quality of the correction can be assessed by comparing the BCG artifact occurrences before and after correction, based on the root mean square (RMS) of the BCG waveform or their peak-to-peak (PTP) values (Chowdhury et al., 2014). Additionally, the total spectral power within windows around the cardiac fundamental frequency and its first harmonics (Liu et al., 2012) can be computed, and a ratio expressing the loss in normalized spectral power after the correction is used to quantify the amount of BCG artifact that was removed, measured by the Improvement in terms of Normalized Power Spectrum (INPS) (Tong et al., 2001).

Many studies continue to be dedicated to the development of more efficient methods for BCG artifact correction, but the associated, unwanted removal of true physiological signal in the background has not been systematically assessed. Here, we propose a novel method for the selection of BCG-related ICs (PROjection onto Independent Components, PROJIC), after which three ICA-based approaches for the removal of the BCG artifact are explored. First, the contribution of the BCG-related ICs is removed in the back-reconstruction step of the EEG signal (PROJIC). Alternatively, we propose the use of OBS (PROJIC-OBS) or AAS (PROJIC-AAS) for correcting the BCG-related ICs before back-projecting them, instead of simply removing their contribution. In parallel, a novel evaluation pipeline that assesses both artifact and background signal removal is presented, and used to compare the novel approaches with previous approaches, on data collected from a group of epilepsy patients (imaged at 3 T) and a group of healthy volunteers (imaged at 7 T). Data quality improvements on ERPs of interest collected with both setups (inter-ictal epileptiform discharges, IEDs, and visual-evoked potentials, VEPs, collected at, respectively, 3 T and 7 T) were also assessed by means of an inter-trial variability measure.

## Materials and methods

The main steps of the processing pipeline proposed in this work for the optimal BCG artifact correction and subsequent evaluation, in terms of not only artifact removal and physiological signal preservation, but also data quality improvements on ERPs of interest collected with both datasets, are depicted in Fig. 1.

### EEG-fMRI Data Acquisition

Two sets of simultaneous EEG-fMRI data were used, which were obtained with two different EEG-fMRI setups, a commercially available, standard one at 3 T and an optimized, custom one at 7 T.

#### Setup #1 (3 T)

A group of twelve patients ( $12 \pm 9$  years old, 7 males/5 females) with drug-refractory focal epilepsy undergoing pre-surgical evaluation

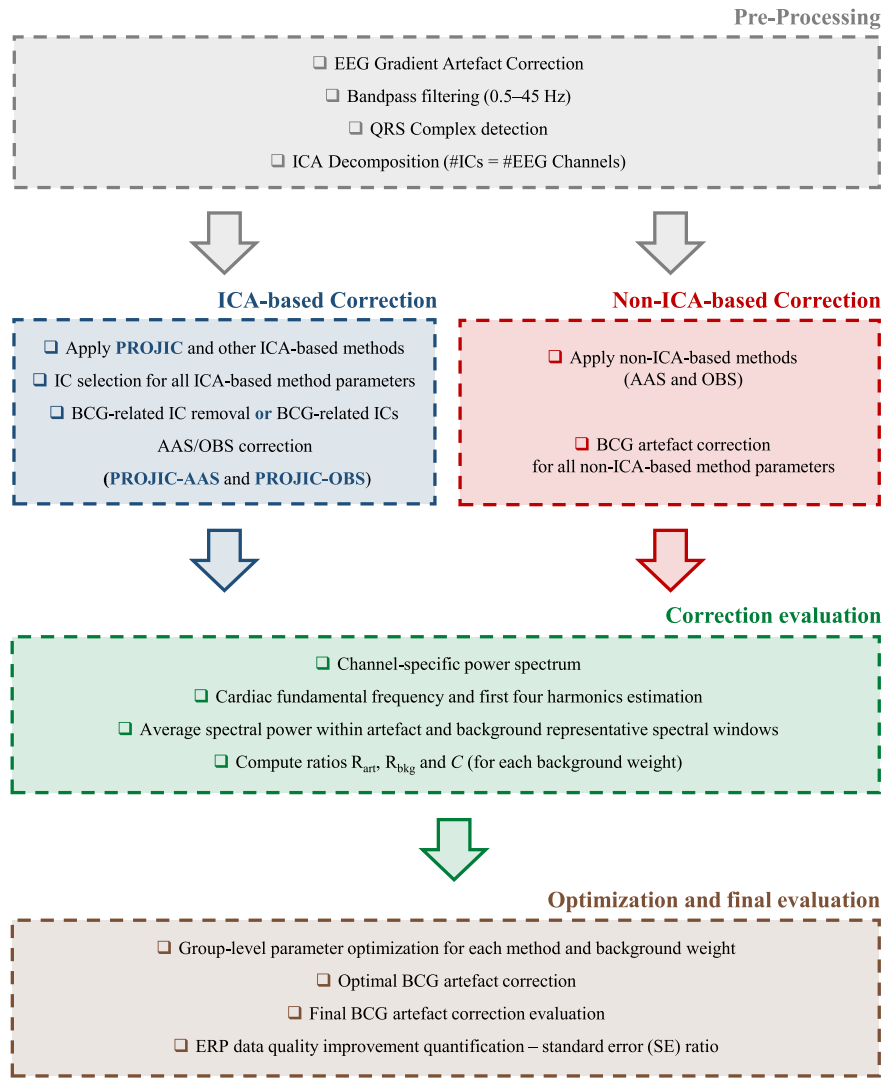


**Fig. 1.** Schematic diagram of the processing pipeline for the optimal BCG artifact correction. 1) EEG data is pre-processed, ICA decomposed and 2) artifact-corrected resorting to different ICA- and non-ICA-based methods. 3) BCG artifact correction is evaluated in the frequency domain, by means of the combination of two ratios reflecting the relative amount of artifact and physiological signal removal. 4) The combined ratio is used for an exhaustive group-level optimization of the algorithms' parameters, providing optimal artifact-corrected EEG data, from which ERP data quality improvements are assessed by the inter-trial variability computed as the relative reduction in the standard error across trials.

was selected from the Program of Surgery for Epilepsy of the Hospital Center of West Lisbon, by the clinical team, at suggestion of the physician responsible for the neurophysiological studies. These patients were studied at the Imaging Center of Hospital da Luz in Lisbon, Portugal. All patients or their legal representatives gave written informed consent and the study was approved by the local ethics committee.

The imaging was performed on a 3 T Siemens Verio scanner (Siemens, Erlangen) using a 12-channel RF receive coil. Functional images were acquired using a 2D multi-slice gradient-echo echoplanar imaging (EPI) sequence, with TR/TE = 2500/30 ms, 37 or 40 contiguous axial slices with interleaved acquisition, and  $3.5 \times 3.5 \times 3.0 \text{ mm}^3$  voxel size, yielding whole-brain coverage in all cases.

EEG data were recorded using an MR-compatible 32-channel BrainAmp MR plus amplifier (Brain Products, Germany). A standard BrainCap MR model (EasyCap, Herrsching, Germany) was used, containing 31 Ag/AgCl ring-type electrodes arranged according to the 10–20 system, a dedicated electrode for the referencing, and one electrode placed on the back for ECG recording. Sampling was performed at 5000 Hz, synchronized with the scanner's 10 MHz clock.

For each patient, two or three simultaneous EEG-fMRI runs of 10 or 20 min were then performed inside the MR scanner, yielding a total of

30 min. For the 12 patients, a total of 26 EEG datasets concurrently acquired with fMRI were collected during rest. IEDs were captured with EEG on 6 out of the 12 patients that participated in this study.

#### Setup #2 (7 T)

A group of six healthy volunteers ( $20 \pm 2$  years old, 5 males/1 female) was studied at the Centre d'Imagerie BioMédicale (CIBM) in Lausanne, Switzerland. This study was approved by the institutional review board of the local ethics committee, and all subjects provided written informed consent.

The imaging was performed on an actively-shielded Magnetom 7 T head scanner (Siemens, Erlangen, Germany), using an 8-channel transmit/receive RF coil (Salomon et al., 2014). For each subject, two simultaneous EEG-fMRI runs, of 5 and 8 mins, respectively, were collected. Functional images were acquired using a 2D multi-slice gradient-echo EPI sequence, with TR/TE = 2000/25, from 25 axial slices, and  $1.5 \times 1.5 \times 1.5 \text{ mm}^3$  voxel size. A visual stimulation was applied in the 5-min run for each subject, according to the functional paradigm described in (Jorge et al., 2015a).

EEG data were recorded using an optimized setup, as described in (Jorge et al., 2015b), using two 32-channel BrainAmp MR Plus amplifiers (Brain Products, Munich, Germany). A customized BrainCap

MR model (EasyCap, Herrsching, Germany) was used, containing 59 Ag/AgCl ring-type electrodes arranged according to the 10–20 system, a dedicated electrode for the referencing, and one electrode placed on the back for ECG recording. Sampling was performed at 5000 Hz, synchronized with the scanner's 10 MHz clock. A total of 11 intra-MR EEG datasets were collected (as one of the subjects did not undergo the 8 min run), 6 of which presented VEPs.

### Data processing

All processing steps were implemented in MATLAB® using in-house software, except for the pre-processing and ICA decomposition of EEG data, which were performed using the EEGLAB toolbox (Delorme and Makeig, 2004). Also, the implementations of AAS and OBS as in the EEGLAB's FMRIB plug-in were used. Except when stated otherwise, the same pre-processing was applied to EEG recordings from both setups. All EEG datasets were gradient artifact-corrected using AAS (Allen et al., 2000), downsampled to 250 Hz and band-pass filtered (0.5–45 Hz). EEG data collected using Setup #1 were volume-wise gradient artifact-corrected since the first artifact occurrence within each TR was considerably different from the remaining ones, in terms of both morphology and duration. Since this was not observed for Setup #2, a slice-wise gradient artifact correction was performed in this case. An average over 100 slice samples was subtracted from each slice: 50 samples from the preceding and 50 samples from the following slices, with jittered steps of 8–13 slices separating the selected samples, allowing for the preservation of low-frequency EEG activity, as well as a balanced distribution of samples relative to the visual stimulation cycle (3.35 Hz) (Jorge et al., 2015a).

The *Infomax* ICA algorithm, as implemented in the EEGLAB toolbox, was then applied to the pre-processed intra-MR EEG data using the default parameters. The ICA algorithm decomposes the  $N \times M$  EEG data into  $L \times M$  independent components (ICs), where  $N$ ,  $L$  and  $M$  denote, respectively, the number of channels, ICs to be estimated and time-samples. The number of components is defined equal to the number of EEG channels: 31 and 59 for data collected using Setups #1 and #2, respectively. In that case, the equation describing the relationship between the EEG signal,  $\mathbf{E}$ , and the independent components,  $\mathbf{I}$ , is given by:

$$\mathbf{I}_{[N \times M]} = \mathbf{W}_{[N \times N]} \cdot \mathbf{E}_{[N \times M]} \quad (1)$$

where  $\mathbf{W}$  represents the *un-mixing matrix* which carries the coefficients of the linear combination between the EEG data and the ICs (Bell and Sejnowski, 1995; Lee et al., 1999).

The detection of QRS complexes on ECG data using Setup #1 was performed using a modified version of the Pan-Tompkins algorithm (Pan and Tompkins, 1985). As for the EEG recordings using Setup #2, no clear R peaks could be visually observed on ECG, nor the typical morphology within each beat. Thus, cardiac triggers were first estimated from the ECG channel and then fine-tuned by a correlation-maximization approach, using a combination of EEG channels where pulse artifacts were most prominent (Jorge et al., 2015a; Mijović et al., 2012). These annotations were centered in the middle of each BCG artifact occurrence. The estimated cardiac triggers were visually inspected for false positives and false negatives.

### BCG Artifact correction

The MATLAB® code for the procedures described in the following sub-sections is available at: [https://github.com/rmabreu/BCG\\_Artifact\\_Correction.git](https://github.com/rmabreu/BCG_Artifact_Correction.git).

### BCG-related IC selection

As a starting point for the BCG-related IC selection, it was hypothesized that only a limited set of ICs is significantly affected by the BCG artifact. Hence, by projecting the BCG waveform onto the IC space, those

components that span the artifact will have higher-powered projections when compared to those that are relatively artifact free. Importantly, the average BCG waveform is expected to be roughly devoid of other large amplitude artifacts (e.g., motion, eye blinks, among others), as those are not time-locked to the heartbeat and thus should be averaged out. For the purpose of computing the average BCG waveform, QRS-triggered event-related potentials (QRS-ERPs) are first computed, using the detected R peaks as time-locking events, yielding an  $N \times E \times T$  matrix, where  $N$  is the number of EEG channels,  $E$  the number of epochs or R peaks and  $T$  the length of each epoch, the latter being dependent on the subjects' cardiac rate. The average across epochs is then computed, yielding the  $N \times T$  matrix  $\mathbf{M} = (\mathbf{m}_1, \dots, \mathbf{m}_N)$ , where  $\mathbf{m}_i$  is the average QRS-ERP of the  $i$ -th channel, of length  $T$ . Considering  $\mathbf{M}$  the aforementioned BCG waveform, a set of  $N$  projections,  $\mathbf{P}$ , of the average QRS-ERP onto the IC space are computed by means of the corresponding un-mixing matrix  $\mathbf{W}$  as:

$$\mathbf{P} = \mathbf{W} \cdot \mathbf{M} \quad (2)$$

The classification of ICs as BCG or non-BCG related is performed by means of a  $k$ -means clustering algorithm. The power of each projection in  $\mathbf{P}$  is computed as the squared sum of each projection occurrence, and used as the discriminative feature to inform the clustering algorithm. The number of clusters to be computed is a mandatory input of  $k$ -means, and it will influence the classification output profoundly. Due to the subsequent parameter optimization step that will be described next, artifact correction using PROJIC is repeated with the number of clusters,  $k$ , ranging from 2 to 5. For each value of  $k$ , the cluster centroids are sorted in descendent order, so that ICs assigned to the first, highest centroid cluster will then yield corresponding projections with the highest power and vice-versa for ICs assigned to the last cluster. As a selection criterion, the ICs labeled as belonging to the first  $k - 1$  clusters (after sorting) are classified as BCG-related. The upper limit for the number of clusters is chosen to ensure that even in this case, all selected ICs still exhibit strong artifact contributions. In fact, the higher the power of a given projection, the larger is the contribution of the BCG artifact to the associated IC, and for higher  $k$ , ICs associated with lower-powered projections are also selected, thus exhibiting only minor contributions of the BCG artifact.

### PROJIC algorithm

A BCG artifact-corrected EEG,  $\mathbf{E}_{cor}$ , is obtained by back-projecting all the ICs except those classified as BCG-related according to:

$$\mathbf{E}_{cor} = \mathbf{X} \cdot \mathbf{Z} \cdot \mathbf{I} \quad (3)$$

where  $\mathbf{Z}$  is a  $N \times N$  diagonal matrix in which the  $z_{ii}$  element is equal to 0 if the  $i$ -th IC was classified as BCG-related, and 1 otherwise.  $\mathbf{X}$  denotes the mixing matrix, that is, the inverse of  $\mathbf{W}$ , representing the spatial map, or topography, associated to each IC and respective time-course (Bell and Sejnowski, 1995; Lee et al., 1999). The contribution of the selected components is then removed, yielding a purely ICA-based BCG artifact-corrected EEG signal.

### PROJIC-OBS and PROJIC-AAS algorithms

As discussed previously, one of the main assumptions of ICA algorithms is the stationarity of the sources, which is not completely fulfilled for the BCG artifact, and rendering the selected ICs potentially contaminated by other contributions of interest. On the other hand, it is expected that the time-courses of the ICs classified as BCG-related should yield artifact occurrences that are closer to the ones of the artifact than those of the original data, since the latter results from a weighted contribution of several head sources, including the BCG artifact ones. Taking these considerations into account, two modified versions of the purely ICA-based PROJIC algorithm are proposed, whereby the ICs classified as BCG-related according to the selection criteria

described previously, are corrected for the BCG artifact occurrences by either applying the OBS (Niazy et al., 2005) (PROJIC-OBS method) or the AAS (Allen et al., 1998) (PROJIC-AAS method) algorithms to the associated time-courses. Instead of simply removing their contribution, the artifact-corrected BCG-related ICs are also included in the back-reconstruction of the EEG signal, attempting to guarantee that physiological EEG variance captured by those ICs is preserved, while suppressing that of the BCG artifact occurrences.

The PROJIC-OBS and PROJIC-AAS algorithms present two parameters that are likely to be optimized: the number of clusters in the IC selection step and, respectively, the number of PCs or artifact windows that will be used to build the artifact template in the IC space. Thus, artifact correction is repeated with the number of clusters ranging from 2 to 10, while the number of PCs in PROJIC-OBS range from 3 (the minimum number of PCs recommended in (Niazy et al., 2005)) and 10, in unit steps. As for the PROJIC-AAS, the number of artifact windows is set to range from 10 to 80, in steps of 10. A more flexible selection of BCG-related ICs was permitted for PROJIC-OBS and PROJIC-AAS by increasing the upper limit of the number of clusters range. In fact, only the artifact-related variance of the selected ICs is expected to be removed, in contrast with PROJIC, for instance, which thus requires a more conservative selection. Hence, ICs less contributed by the artifact may be selected for higher number of clusters. All possible combinations of parameters are tested, yielding a total of  $9 \times 8 = 72$  artifact-corrected EEG traces for both PROJIC-OBS and PROJIC-AAS algorithms.

#### Comparison with state-of-the-art methods

Several criteria for the selection of BCG-related ICs can be found in the literature, and reviewed in (Vanderperren et al., 2010). Here, we tested the following methods, repeating the analysis with varied parameters within reasonable intervals, which will be then optimized in the subsequent optimization step:

- 1. Correlation.** Each IC time-course is first correlated with the simultaneously acquired ECG signal (CorrECG method) (Mantini et al., 2007; Srivastava et al., 2005). Alternatively, a template for the BCG artifact is computed by detecting the artifact occurrences, concatenating them and averaging across channels (CorrBCG method) (Srivastava et al., 2005). The correlation coefficients are used as threshold for the selection of ICs. The threshold ranges from 0.05 to 0.35, in 0.05 steps, 0.2 being the default (Vanderperren et al., 2010).
- 2. Auto-correlation (AutoCorr method).** The auto-correlation of each IC time-course is computed, searching for the ones with a peak in the auto-correlation function located at the distance between two consecutive QRS complexes (Deburghraeve et al., 2008). ICs yielding an estimated fundamental frequency located no more than 2.5% to 27.5% (in 5% steps) away from the cardiac frequency are classified as BCG-related. The default is 10%. This value was empirically determined, as no references in the literature were found.
- 3. Frequency content (PSD method).** The presence of BCG artifacts is characterized by high-amplitude peaks in the power spectrum of EEG data at frequencies next to the cardiac fundamental frequency and its first harmonics. The power spectrum of each IC can thus be probed for a higher average spectral power within those frequency windows, possibly indicating the presence of a BCG-related IC (Vanderperren et al., 2007). After normalizing and sorting in descending order the average spectral power of each IC, the first ICs yielding a minimum of 10% to 50% (in 5% steps) of the cumulative average spectral power are classified as BCG-related ICs. The default is 40%. This value was empirically determined, as no references in the literature were found.
- 4. Variance explained (VE method).** The amount of variance explained (VE) by each source to the occurrence of BCG artifacts is used to determine whether an IC is BCG-related or not (Debener et al., 2008), as a threshold ranging from 0.025 to 0.275, in 0.05 steps. The default is 0.1 (Vanderperren et al., 2010).

- 5. Peak-to-peak of reconstructed sources (BackProj method).** It is assumed that, when individually back-projecting a given BCG-related IC onto the EEG space, the reconstructed EEG signal will exhibit peaks at times of BCG artifact occurrences. The difference between the maximal and minimal peak-to-peak (PTP) values of the QRS-ERP is computed for each channel. The relative contribution of a source is quantified by computing the ratio between the PTP differences of both reconstructed and original EEG signals (Vanderperren et al., 2010). The normalized PTP is used as threshold, ranging from 0.01 to 0.50, in 0.05 steps. The default is 0.25 (Vanderperren et al., 2010).

The ICs classified as BCG-related based on the different selection criteria are removed from the back-reconstruction step of the EEG signal according to Eq. (3), yielding purely ICA-based corrections.

A comparison with other previous, non-ICA-based approaches was also performed, comprising the two most commonly used methods, AAS and OBS. For the purpose of assessing the performance of these methods, as well as the effect of parameter optimization, artifact correction is repeated with the number of windows used to compute the average template in AAS set to 20, 30 or 40 (20 being the default (Delorme and Makeig, 2004)); the number of PCs in OBS is set to 3, 4 or 5 (4 being the default (Delorme and Makeig, 2004; Niazy et al., 2005)). Prior to correction, a fixed time delay is applied to the cardiac triggers as needed in order to have them placed at the center of each artifact occurrence.

#### BCG Artifact correction evaluation

Two frequency-based ratios reflecting the performance of the BCG artifact correction methods in terms of artifact removal and background physiological signal preservation are defined as:

$$R_{art} = \frac{S_{art}^{unc} - S_{art}^{cor}}{S_{art}^{unc}}, \quad R_{bkg} = \frac{S_{bkg}^{unc} - S_{bkg}^{cor}}{S_{bkg}^{unc}} \quad (4)$$

where  $S_{art}^{unc}$  and  $S_{art}^{cor}$  denote the average spectral power before and after BCG artifact correction, respectively, within representative windows of artifact. Analogously,  $S_{bkg}^{unc}$  and  $S_{bkg}^{cor}$  denote the average spectral power before and after BCG artifact correction, respectively, within representative windows of physiological background. While  $R_{art}$  quantifies the percentage of BCG artifact that is removed and hence should be maximized,  $R_{bkg}$  quantifies the relative amount of physiological background that is removed from EEG data and hence should be minimized. The procedure used to obtain the representative windows of artifact and physiological background is described next.

First, the Fast Fourier Transform (FFT) of the EEG signal before and after applying the different correction methods is obtained. Since the timing of the BCG artifact is closely related to the occurrence of the R peaks in the ECG signal, it is expected that BCG-contaminated EEG data will yield spectral peaks at cardiac-related frequencies. For the purpose of defining artifact representative windows, an approximation of the cardiac fundamental frequency,  $f_0$ , and its first four harmonics  $f_n = (n + 1) \times f_0$ , with  $n = 1, 2, 3, 4$ , is first obtained based on the heart rate. The exact value of  $f_n$ , however, is determined by convolving a Lorentzian function of width 0.01 Hz and radius 0.3 Hz with power spectrum windows of 0.1 Hz centered in  $f_n$ , and extracting the convolution peaks (Rothlübbers et al., 2014). In order to guarantee that the quantification of the BCG artifact reduction is computed only in ECG harmonics for which a BCG-related peak in the power spectrum is present, the value of the convolution peaks is used as a rejection criterion. The harmonics yielding a convolution value lower than 25% of the maximum across all harmonics and channels are discarded from the subsequent quantification, avoiding an underestimation of the BCG artifact contribution. A threshold of 20% is used for the EEG recordings in Setup #2, taking into account the higher variability of convolution peaks across channels

and datasets in this case. The convolution thresholds were empirically determined. The artifact representative windows are finally defined as 0.13 Hz windows centered in the cardiac harmonics exhibiting a spectral peak according to the criterion described previously (Fig. 2).

Physiological background is quantified within a 0.39 Hz window centered in a frequency 0.52 Hz above each BCG artifact window (Fig. 2). For the purpose of taking into account the dips in the power spectrum at frequencies around the TR of the fMRI acquisition, associated with residuals of the application of the gradient artifact correction algorithm, 0.04 Hz windows centered at the TR-related frequencies are defined and their contribution excluded from the subsequent computations. Thus, an underestimation of the average spectral power for both BCG correction and background preservation is avoided.

#### Parameter optimization procedure

Depending on the final goal of a given study, one might be interested in removing as much as possible of the BCG artifact without being too much concerned with the preservation of the physiological background signal (e.g., ERP studies); in resting-state studies, however, where no ERPs are present in EEG data, preserving the physiological background signal is of utmost importance at a cost of leaving residual BCG artifact contributions. Taking into account these potential trade-offs, a combined ratio,  $C$ , is defined:

$$C(w_{bkg}) = w_{bkg}(1 - R_{bkg}) + (1 - w_{bkg})R_{art} \quad (5)$$

where  $w_{bkg}$  denotes the physiological background weight reflecting the importance given to the preservation of the EEG background signal in relation to the removal of the BCG artifact. By varying  $w_{bkg}$  from 0 (the BCG artifact removal is the priority) to 1 (the physiological background signal preservation is the priority) in steps of 0.1, an exhaustive search optimization algorithm is employed for each value of  $w_{bkg}$ . For the PROJIC algorithm, Eq. (5) can be written as:

$$C(w_{bkg}, k) = w_{bkg}(1 - R_{bkg}(k)) + (1 - w_{bkg})R_{art}(k) \quad (6)$$

The optimization algorithm aims at finding the optimal number of clusters,  $k^*$ , that maximize  $C$  for each value of  $w_{bkg}$ , according to:

$$k^*(w_{bkg}) = \arg \max_k C(w_{bkg}, k) \quad (7)$$

When combining PROJIC and OBS, Eq. (5) can be written as:

$$C(w_{bkg}, k, p) = w_{bkg}(1 - R_{bkg}(k, p)) + (1 - w_{bkg})R_{art}(k, p) \quad (8)$$

where  $p$  denotes the number of PCs used to build the optimal basis set that will be used to remove the artifact occurrences from the BCG-related ICs. The optimization algorithm sequentially searches for the optimal number of PCs and clusters,  $(k^*, p^*)$ , that maximize  $C$  for each value of  $w_{bkg}$ , according to:

$$(k^*, p^*)(w_{bkg}) = \arg \max_{k, p} C(w_{bkg}, k, p) \quad (9)$$

Eqs. (8–9) can be easily adaptable for the PROJIC-AAS algorithm, by replacing  $p$  with  $w$ , where  $w$  denotes the number of artifact windows used to build the average artifact template that will be subtracted from the data.

A subject-specific optimization of the method parameters was first performed. Interestingly, the optimal parameters were not found to substantially differ across subjects, exhibiting between-subjects coefficients of variation of 21.7% and 19.9%, averaged across methods and background weights, for data collected at 3 T and 7 T, respectively. Based on this relatively modest variability, a group-level optimization was then conducted and statistically significant differences were not found ( $p > 0.05$ ) between the performances of each method, when performing the optimization on a subject- or group-level. Because the same setup-specific set of optimized parameters is therefore used for all EEG datasets and subjects, straightforward and general conclusions and recommendations can be drawn for each setup.

#### Method comparison

All proposed approaches, PROJIC, PROJIC-OBS and PROJIC-AAS, were compared to other purely ICA-based methods described in Section 2.3.4, as well as with the non-ICA-based methods AAS and OBS, in terms of the ratios  $C$  computed for all background weights. Similarly to newly proposed methods, all other correction algorithms tested were submitted to a group-level optimization of their respective parameters. The optimization procedure is partially motivated by previous studies reporting that the use of default parameters when applying AAS or OBS for BCG artifact removal might not yield reasonable results in all cases, particularly on data collected at 7 T (Debener et al., 2008). In order to assess the impact of the parameter optimization on the novel methods, the following

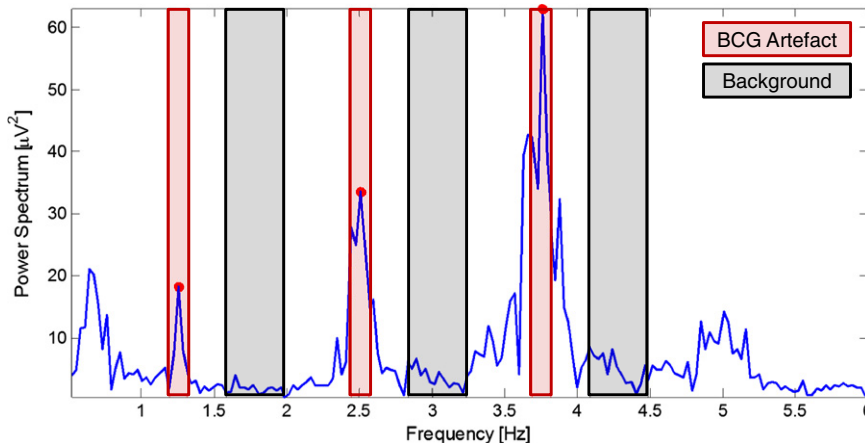


**Fig. 2.** Power spectrum of a highly BCG artifact-contaminated EEG channel, for a representative subject imaged using Setup #1 at 3 T: illustration of the frequency windows used for the evaluation of the artifact and background physiological signal removal. The red rectangles show power spectrum windows of 0.13 Hz around  $f_0$  and the first two harmonics of the ECG signal. The associated spectral peaks (highlighted by the red circles) exhibited a relative convolution value higher than 25% of the maximum across all harmonics and channels, thus contributing to the quantification of  $S_{diff}^{BKG}$ . The black rectangles denote the corresponding power spectrum windows associated with the background.

sets of default parameters were defined: PROJIC,  $k = 2$ ; PROJIC-OBS,  $(k, p) = (4, 4)$ ; PROJIC-AAS,  $(k, w) = (4, 20)$ . The most conservative scenario was considered as default for PROJIC; the default set of parameters for PROJIC-OBS and PROJIC-AAS was chosen based on a fairly conservative selection of BCG-related ICs, allowing for the selection of ICs less contributed by the artifact, and followed by the default parameters of OBS and AAS, respectively (Delorme and Makeig, 2004; Niazy et al., 2005).

The main effects of the optimization procedure, the method used for the BCG artifact removal and the background weights, as well as interaction effects, were evaluated by means of a 3-way repeated measures Analysis of Variance (ANOVA) for the combined ratio C. Multiple comparisons using 1-way ANOVA between the correction methods were performed by means of a post-hoc statistical test with the Tukey–Kramer correction. A level of significance  $p < 0.05$  was considered.

### ERP Quality assessment

The impact of the BCG correction on the quality of the ERPs of interest recorded with Setups #1 and #2 (IEDs and VEPs, respectively) is quantified by means of an inter-trial variability measure (Niazy et al., 2005). For EEG data collected using Setup #1, the IEDs were visually inspected by an expert neurophysiologist and subjected to a standard alignment step, by shifting them to match the occurrence of a negative peak, which was observed in all IED types recorded. The aligned annotations are then used as time-locking events to epoch the EEG data. The duration of the epochs is defined for each patient separately, taking into account the inherent variability across IEDs due to the patients' heterogeneous epilepsy profiles. Regarding Setup #2, the VEP onsets were provided by a photodiode sensor placed in front of the LCD projector (Jorge et al., 2015a). The duration of each epoch is defined as the

average difference between successive VEP onsets. In both setups, EEG data are re-referenced to the average channel and band-pass filtered: 1–45 Hz for Setup #1 and 3–40 Hz for Setup #2 (Jorge et al., 2015a).

The relative reduction in the standard error ( $R_{SE}$ ) across trials, before ( $SE_{unc}$ ) and after ( $SE_{cor}$ ) applying the different BCG artifact correction methods tested, is computed as:

$$R_{SE} = \frac{SE_{unc} - SE_{cor}}{SE_{unc}} \quad (10)$$

$R_{SE}$  should always be positive, as it is expected a lower inter-trial variability after correcting EEG data for the BCG artifact under the assumption that the artifact occurrences are uncorrelated with the ERPs of interest (Niazy et al., 2005; Vanderperren et al., 2010). This performance metric is calculated for each EEG channel, subject, correction method and background weight. The specific set of optimized parameters for each background weight and method is used (obtained according to the procedure described in 2.4).  $R_{SE}$  is finally averaged across channels and subjects.

### Results

The results obtained using the different algorithms tested on the data collected using Setups #1 and #2 are presented and discussed jointly in this section. The IC selection criterion underlying PROJIC was found to successfully select BCG-related ICs in both setups, as evidenced by the clear presence of artifact occurrences in the corresponding time-courses upon direct visual inspection. Moreover, the subsequent application of the three proposed approaches was also found to substantially reduce the BCG artifact from the EEG data. Illustrative examples of ECG, EEG and IC time courses (Figs. 3 and 4), the EEG power spectrum (Figs. 5

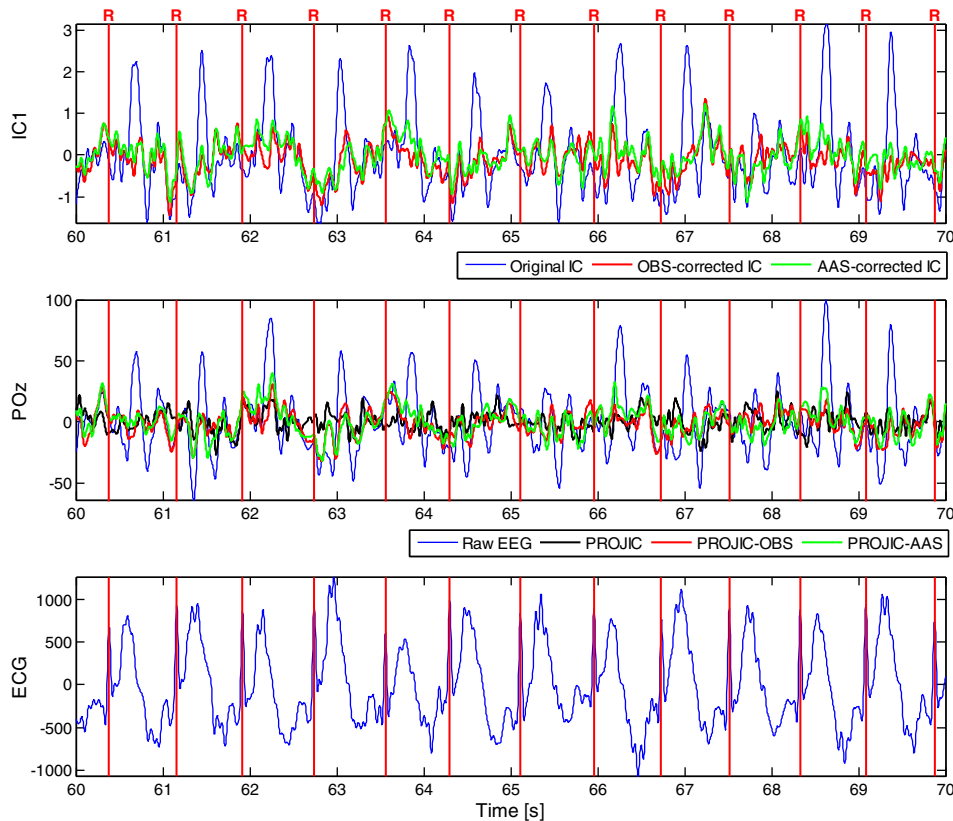


**Fig. 3.** Illustration of the PROJIC, PROJIC-OBS and PROJIC-AAS algorithms for data collected using Setup #1 at 3 T: segments of 10 s from the BCG-related IC #1 (top), EEG channel POz (middle) and the corresponding ECG signal (bottom), for a representative subject with an average heart rate of approximately 75 BPM. The BCG artifact occurrences were greatly attenuated with OBS and AAS, yielding the BCG artifact corrected EEG channel POz, highlighted by the red and green traces, respectively. In black, the output of the purely ICA-based PROJIC algorithm is illustrated. PROJIC, PROJIC-OBS and PROJIC-AAS algorithms were optimized for  $w_{bkg} = 0.5$ , yielding the optimal parameters  $k^* = 3$ ,  $(k^*, p^*) = (10, 3)$  and  $(k^*, p^*) = (10, 10)$ , respectively.

and 6) and the evaluation ratios spatial distribution for  $w_{bkg} = 0.2, 0.5$  (Figs. 7 and 8) are provided for Setups #1 and #2, respectively. The group average values of the ratio  $C$  (Eq. (5)) as a function of background weight, for all methods tested, are shown in Figs. 9 and 10. Illustrative ERPs and the average inter-trial variability across subjects as a function of background weight, before and after correction with the different methods tested, are shown in Figs. 11 and 12.

In Figs. 3 and 4, the BCG-related IC time-course yielding the highest-powered projection, the highly BCG artifact-contaminated EEG signal from the POz and Oz channels and the corresponding ECG signal are shown for representative subjects. The BCG artifact occurrences in the ICs #1 (Fig. 3) and #2 (Fig. 4) time-courses were greatly suppressed when using PROJIC-OBS and PROJIC-AAS. A clear attenuation of the BCG artifact is observed for all methods. For Setup #1, artifact residuals are present if either PROJIC-OBS or PROJIC-AAS methods are applied; however, physiological fluctuations in between BCG artifact occurrences are less attenuated as well (Fig. 3). In contrast, for Setup #2, PROJIC and PROJIC-OBS seemed to better preserve physiological fluctuations without clearly compromising the reduction of the BCG artifact in this case (Fig. 4).

In Figs. 5 and 6, the power spectra of the EEG signal from POz and Oz channels are shown before and after applying all the correction methods tested, for Setups #1 and #2, respectively. While only the harmonics  $f_0$  and  $f_1$  of the ECG signal were deemed to present a clear spectral peak in the POz channel (Setup #1), the quantification of the BCG artifact removal and physiological signal preservation was based on all harmonics except for  $f_4$  in the Oz channel (Setup #2). When comparing the three novel methods, the attenuation in power near cardiac-related frequencies was found to be comparable, with a stronger reduction from PROJIC-AAS observed for both setups. The OBS and

PROJIC algorithms yielded the strongest reduction of the power spectrum amplitude in general for, respectively, Setups #1 and #2, particularly within physiological background related frequencies, as highlighted by the zoomed background windows. In contrast, the associated, remaining methods seemed to preserve most of the background spectral power.

In Figs. 7 and 8, topographies of both artifact ( $R_{art}$ ) and background ( $1 - R_{bkg}$ ) ratios obtained using all novel and non-ICA-based methods are shown, highlighting the relative reduction in average spectral power of artifact and background signals, averaged across patients, for each channel separately. Although 59-channel EEG acquisitions were performed using Setup #2, only the 31 channels that were also present in the lower-density EEG recordings of Setup #1 are shown, for comparison and visualization purposes. A low inter-subject variability was found for all correction methods and background weights showed here, as evidenced by the blue to dark-blue standard error (SE) topographies for both ratios. As shown in both figures, although more clearly observed for Setup #2 (Fig. 8), the ratios topographies follow a crown-like lateral-posterior pattern, in which electrodes located on the right-left temporal, posterior and frontal-central regions are the most contaminated with the BCG artifact (Debener et al., 2008; Iannotti et al., 2014), thus exhibiting higher values of  $R_{art}$ . As expected, increasing  $w_{bkg}$  yielded lower artifact removal efficiency but also increased the background signal preservation.

The average performance results are shown in Figs. 9 and 10 for Setups #1 and #2, respectively. The combined ratio  $C$  is shown for all methods, before and after the optimization procedure, comparing the three proposed methods with all the ICA-based methods and with AAS and OBS. Significant main effects were found for all factors. Significant interactions were also found between all factors. For Setup

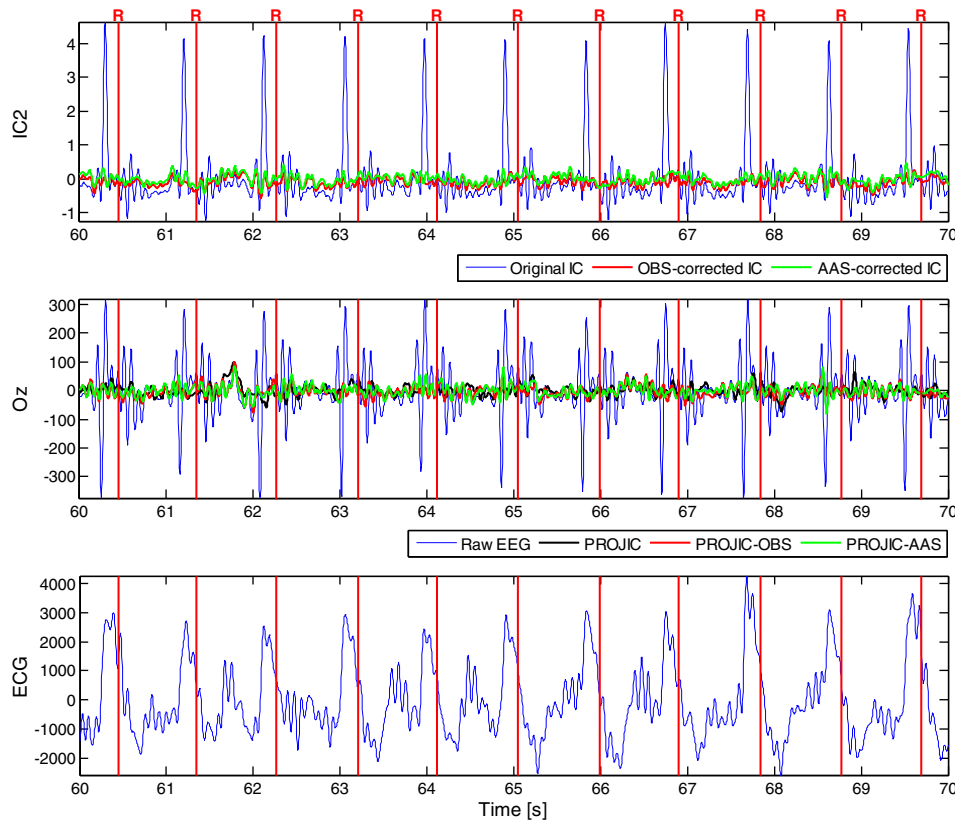


**Fig. 4.** Illustration of the PROJIC, PROJIC-OBS and PROJIC-AAS algorithms for data collected using Setup #2 at 7 T: segments of 10 s from the BCG-related IC #2 (top), EEG channel Oz (middle) and the corresponding ECG signal (bottom), for a representative subject. The high-amplitude BCG artifact occurrences were accurately attenuated with OBS and AAS, yielding the BCG artifact corrected EEG channel Oz, highlighted by the red and green traces, respectively. In black, the output of purely ICA-based PROJIC algorithm is illustrated. PROJIC, PROJIC-OBS and PROJIC-AAS algorithms were optimized for  $w_{bkg} = 0.5$ , yielding the optimal parameters  $k^* = 3$ ,  $(k^*, p^*) = (10, 3)$  and  $(k^*, w^*) = (10, 10)$ , respectively.

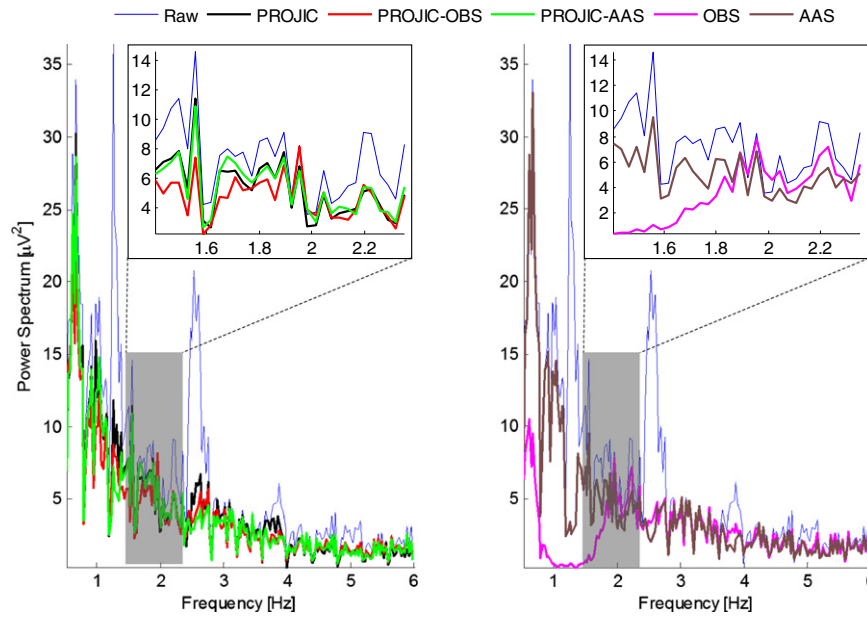


**Fig. 5.** Power spectra of the EEG signal from POz channel, before and after applying the different methods for BCG artifact correction, optimized for  $w_{bkg}=0.5$ , for a representative subject imaged using Setup #1 at 3 T. (A) PROJIC, PROJIC-OBS and PROJIC-AAS exhibited comparable attenuations in power, with the latter further reducing the spectral power within windows around  $f_n$ . (B) OBS yielded the overall strongest attenuation in power. The zoomed, gray background windows highlight the physiological signal removal of each method, with OBS exhibiting the highest spectral power reduction. Small attenuation is observed when using PROJIC and PROJIC-AAS, as the associated power spectrum is comparable to that of raw EEG.

#1, the PROJIC algorithm only outperformed the other ICA-based methods for  $w_{bkg}=0.6, 0.7$ , when considering the optimized parameters. When optimized, VE exhibited the best performance for  $w_{bkg} \leq 0.2$ , BackProj for  $w_{bkg}=0.3, 0.4$ , PSD for  $w_{bkg}=0.5$  and AutoCorr for  $w_{bkg} \geq 0.8$ . Regarding the comparison with the non-ICA-based approaches, after optimization, the PROJIC-OBS algorithm outperformed all methods for  $w_{bkg} \leq 0.2$ . The optimized AAS method achieved the best performance for  $0.7 \leq w_{bkg} \leq 0.9$ , being outperformed by PROJIC-AAS for the remaining background weights. Post-hoc

statistical testing revealed that PROJIC-OBS and PROJIC-AAS were not statistically significantly different from the conventional methods (AAS and OBS).

For Setup #2, the PROJIC algorithm only outperformed the other ICA-based methods for  $w_{bkg}=0.5, 0.6$ , independently from the optimization procedure. When using the optimized parameters, PSD exhibited the best performance for  $w_{bkg} \leq 0.4$ , AutoCorr for  $w_{bkg}=0.7$ , VE for  $w_{bkg}=0.8, 0.9$  and CorrBCG for  $w_{bkg}=1$ . Regarding the comparison with the non-ICA-based approaches, with the optimization procedure, the

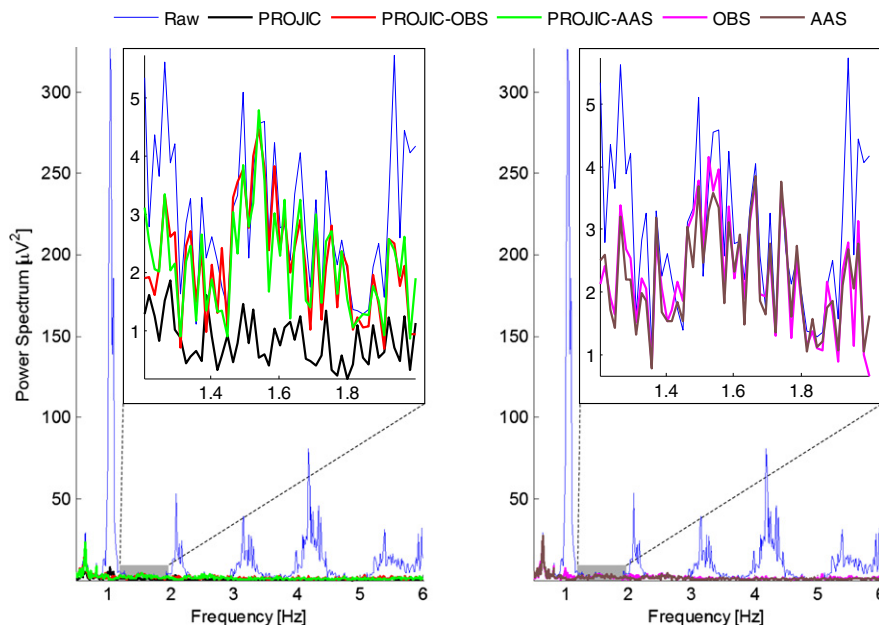


**Fig. 6.** Power spectra of the EEG signal from Oz channel, before and after applying the different methods for BCG artifact correction, optimized for  $w_{bkg}=0.5$ , for a representative subject imaged using Setup #2 at 7 T. (A) PROJIC-OBS and PROJIC-AAS exhibited comparable attenuations in power, with PROJIC-AAS algorithm further reducing the spectral power within windows around  $f_n$ . PROJIC provided the strongest background attenuation, evidenced by the black trace in the zoomed, gray background window. This is not observed for PROJIC-OBS or PROJIC-AAS. (B) AAS yielded the strongest attenuation in power, particularly at cardiac-related frequencies. The zoomed, gray background windows highlight the physiological signal removal of each method, with AAS and OBS exhibiting substantial background signal preservation, as the associated power spectra are quite similar to that of raw EEG.

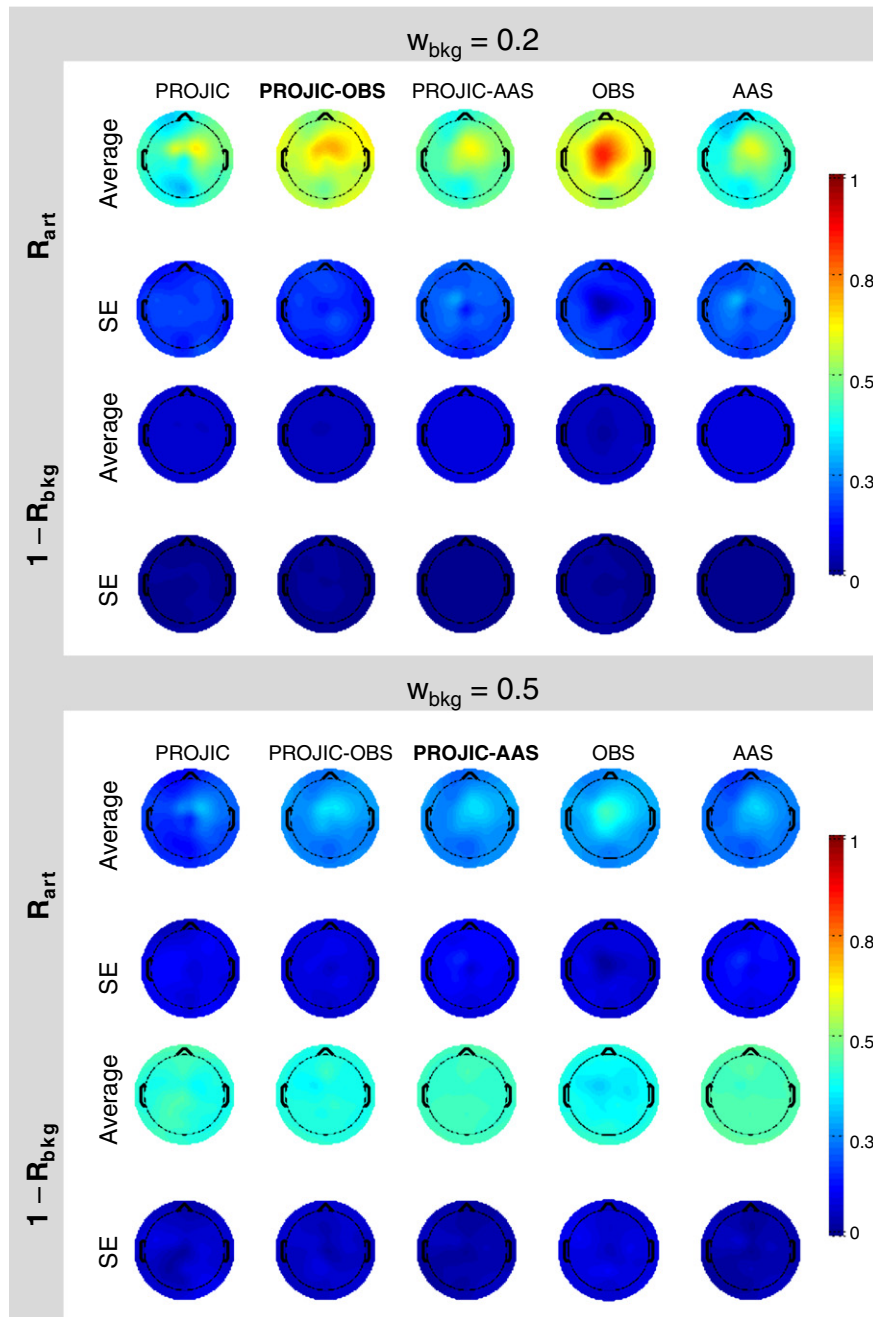


**Fig. 7.** Topographies of artifact ( $R_{art}$ ) and background ( $R_{bkg}$ ) ratios for  $w_{bkg} = 0.2, 0.5$ , after BCG artifact correction by the novel and non-ICA-based methods, averaged across subjects imaged using Setup #1 at 3 T. When mainly driven by the artifact removal ( $w_{bkg} = 0.2$ ), most of the channels exhibited high/low  $R_{art}/R_{bkg}$ , particularly OBS, providing the overall strongest artifact and background removal. OBS was followed by PROJIC-OBS, PROJIC-AAS, PROJIC and finally AAS, the latter providing the most conservative artifact correction. The discrepancy is softened for  $w_{bkg} = 0.5$ , with most of the EEG channels yielding lower/higher  $R_{art}/R_{bkg}$ . The SE topographies reveal a low inter-subject variability across both ratios. The optimal method for the associated background weight is highlighted in bold.

PROJIC-OBS algorithm outperformed all methods for  $w_{bkg} \leq 0.1$ , being surpassed, however, by the OBS algorithm for  $w_{bkg} = 0.2$ . For  $w_{bkg} \geq 0.3$ , the PROJIC-AAS algorithm exhibited the highest values of C, following the same pattern as in the non-optimized methods. The performance of PROJIC-OBS was not significantly different from those of PROJIC-AAS, OBS and AAS. Moreover, PROJIC-AAS was not statistically significantly different from AAS.

Multiple comparisons between all correction methods are depicted in Tables 1 and 2, for data collected using Setups #1 and #2, respectively. PROJIC-OBS, PROJIC-AAS and AAS outperformed all methods for background weights of 0.2 (light gray), 0.5 (gray) and 0.8 (dark gray), respectively, in terms of combined ratio C. On the other hand, OBS

outperformed all methods for  $w_{bkg} = 0.2$  (light gray), while PROJIC-AAS exhibited the best performance for  $w_{bkg} = 0.5, 0.8$  (gray and dark gray, respectively), in terms of the combined ratio C.

The data quality improvements on IEDs and VEPs recorded in subjects that were imaged at 3 T and 7 T are illustrated in Figs. 11 and 12, respectively, in terms of inter-trial variability. The top panel (Figs. 11A and 12A) shows a representative average IED/VEP from P7/POz channel (in red), across epochs, and the associated standard deviation/error, evidenced by the gray area. The standard deviation, instead of the standard error, is illustrated for data collected at 3 T for visualization purposes, in order to make more obvious the effects of the artifact correction methods on IED quality. These channels were selected as

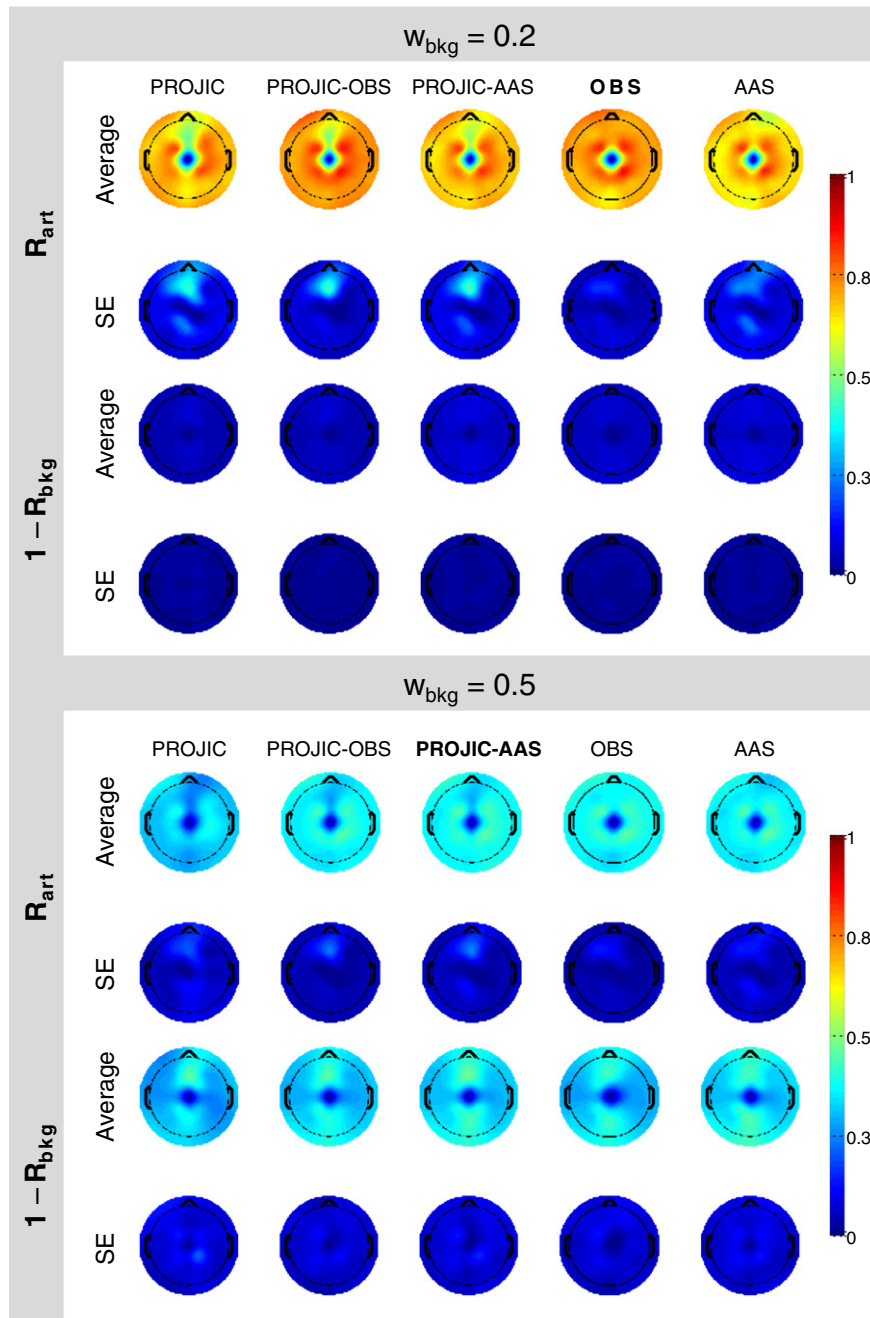


**Fig. 8.** Topographies of artifact ( $R_{art}$ ) and background ( $R_{bkg}$ ) ratios for  $w_{bkg} = 0.2, 0.5$ , after BCG artifact correction by the novel and non-ICA-based methods, averaged across subjects imaged using Setup #2 at 7 T. When mainly driven by artifact removal ( $w_{bkg} = 0.2$ ), most of the channels and correction methods exhibited high/low  $R_{art}/R_{bkg}$ , particularly OBS, in agreement with the findings for Setup #1 (Fig. 7). The discrepancy is softened for  $w_{bkg} = 0.5$  with most of the EEG channels yielding lower/higher  $R_{art}/R_{bkg}$ , without strongly compromising artifact removal over background signal preservation or vice-versa. Similarly for Setup #1, the SE topographies reveal a low inter-subject variability across both ratios. The optimal method for the associated background weight is highlighted in bold.

they provided the average ERPs of the highest amplitude. Consistently across setups, all methods returned comparable results, with PROJIC-OBS and OBS exhibiting a clearer improvement on ERP quality. Particularly, all methods were able to recover the expected features of the more subtle VEP response (when compared to IEDs): the larger P100 component, and the more subtle N75 and N140 components. The PROJIC algorithm, however, introduced unexpected higher-frequency oscillations after the P100 component, without apparent physiological meaning. In Figs. 11B and 12B, the average SE ratio,  $R_{SE}$ , is shown for each method and background weight. The asterisk denotes the optimal method for a given background, considering the combined ratio  $C$ . Only PROJIC-OBS,

when applied to data collected at 3 T, exhibited the best performance in terms of  $C$  and  $R_{SE}$  simultaneously, for  $w_{bkg} \leq 0.2$ .

### Discussion

In this paper, a novel method for the selection of BCG-related ICs was proposed, following which three ICA-based approaches for BCG artifact removal were explored on EEG data recorded simultaneously with fMRI. These novel methods were compared with other ICA-based approaches in the literature, as well as with the commonly used AAS and OBS methods. We found that group-level optimization of the

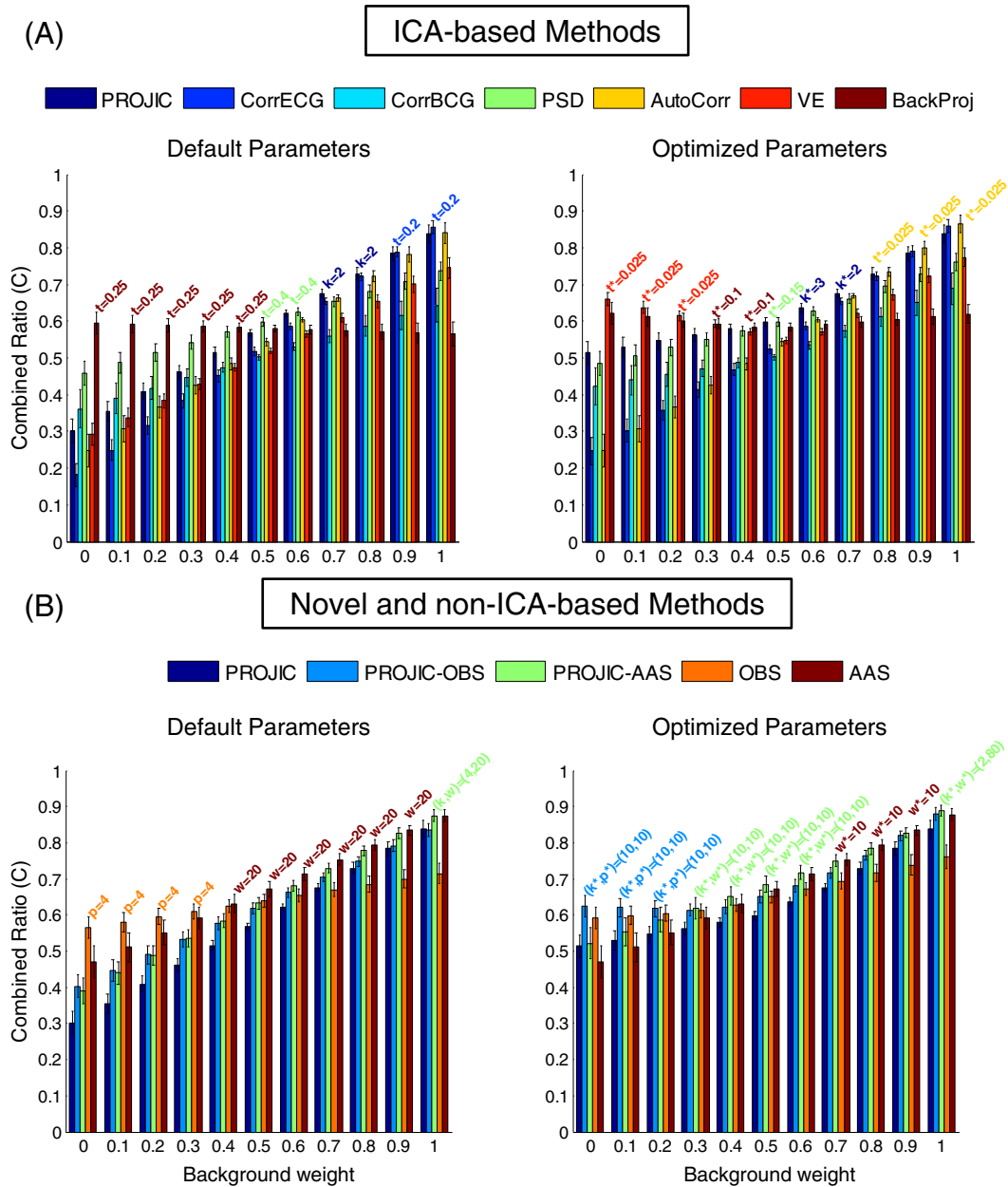


**Fig. 9.** Combined ratios ( $C$ ) for all methods, before and after optimization, for EEG recordings using Setup #1 at 3 T. The optimal method and associated parameters are highlighted, for each background weight. The variability of  $C$  is expressed in terms of the standard error across subjects. (A) PROJIC only surpassed the other ICA-based methods for  $w_{bkg} = 0.7, 0.8$  and  $w_{bkg} = 0.6, 0.7$ , respectively, when considering the default and optimized parameters. (B) If the default parameters are used for each method, OBS outperforms all methods for  $w_{bkg} \leq 0.3$ , being surpassed by AAS for  $0.4 \leq w_{bkg} \leq 0.9$ . When considering the highest background weight, PROJIC-AAS performs better. When submitted to the optimization procedure, PROJIC-OBS yielded the best performance for  $w_{bkg} \leq 0.2$ , being outperformed by the optimized AAS for  $0.7 \leq w_{bkg} \leq 0.9$ . The PROJIC-AAS outperformed every other method for the remaining background weights.

algorithms' parameters significantly improved performance of all methods, and that, when optimized, PROJIC-OBS, PROJIC-AAS and AAS in general outperform all other methods, with PROJIC-AAS exhibiting the best results across the widest range of physiological noise preservation levels. Data quality improvements on ERPs of interest (IEDs and VEPs collected at, respectively, 3 T and 7 T) were also consistently observed with BCG artifact correction, in terms of the relative reduction in the standard error across trials.

#### Method comparison

We found that the performance of the various methods tested is strongly dependent on the relevance given to the preservation of the

physiological signal in the background, relative to the removal of the BCG artifact. In (Grouiller et al., 2007), it was found that AAS was the method of choice whenever high quality ECG data was available, since a poor QRS detection strongly influenced its performance. This is in agreement with our findings, where the AAS algorithm outperformed every other method for some intermediate background weights. Interestingly, the method exhibiting the best performance across most of the background weights was the PROJIC-AAS, which corrects the ICs classified as BCG-related resorting to the AAS algorithm. We further concluded that, for the lowest background weights, the PROJIC-OBS algorithm should be used with the optimal parameters  $(k^*, p^*) = (10, 10)$ , while PROJIC-AAS might be the most suitable method for intermediate and higher background weights.

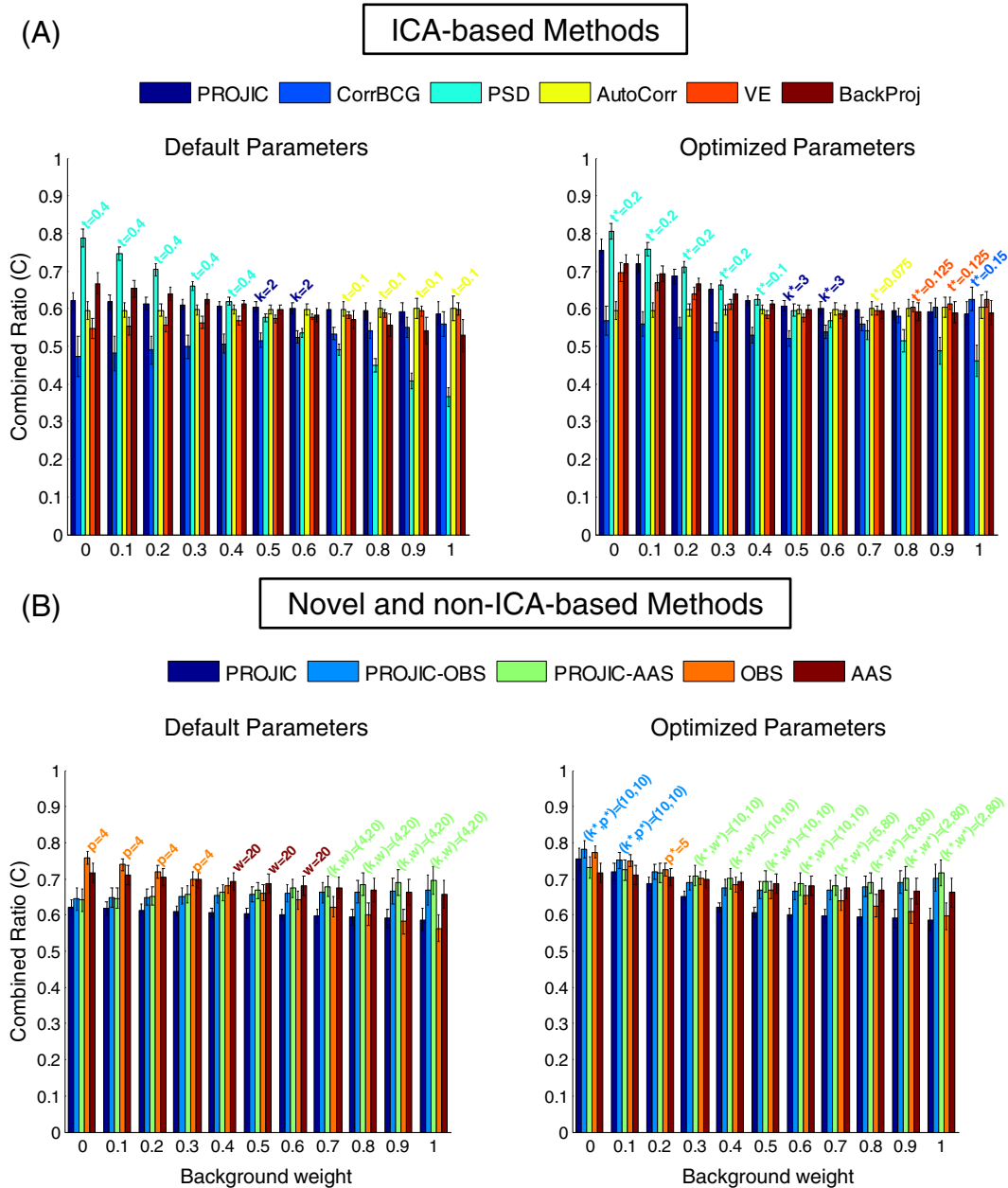


**Fig. 10.** Combined ratios ( $C$ ) for all methods, before and after optimization, for EEG recordings using Setup #2 at 7 T. The optimal method and associated parameters are highlighted, for each background weight. The variability of  $C$  is expressed in terms of the standard error across subjects. (A) Regardless of the optimization procedure being performed, PROJIC only surpasses the other ICA-based methods for  $w_{bkg} = 0.5, 0.6$ . (B) When using the default parameters of each method, OBS outperforms all methods for  $w_{bkg} \leq 0.3$ , being surpassed by AAS when considering  $0.4 \leq w_{bkg} \leq 0.6$ . For the remaining background weights, PROJIC-AAS yielded the best performance, exhibiting the highest values of  $C$ . When submitted to the optimization procedure, substantial increases in  $C$  were observed for all correction methods, with PROJIC-OBS yielding the best performance for  $w_{bkg} = 0, 0.1$ , being outperformed by the optimized OBS for  $w_{bkg} = 0.2$ . The PROJIC-AAS surpassed all the other methods for  $w_{bkg} \geq 0.3$ .

The rationale for correcting the IC time-courses for artifact occurrences has been previously proposed by (Liu et al., 2012). This approach, however, seems mainly focused on removing as much of the artifact as possible, since the BCG-related ICs are removed from the back-reconstruction step of the EEG signal, prior to artifact-correcting all the other ICs. Our approach is rather targeted at keeping intact as much of the physiological background as possible without compromising artifact removal efficiency, by correcting only the BCG-related ICs, and still keeping those for the reconstruction. Although OBS or AAS algorithms are being applied to a presumably time-independent source resulting from the ICA decomposition of EEG data, the BCG artifact variability is still present, as evidenced by the eigenvalues of each PC when applying PCA to the QRS-epoched time-courses of the selected

BCG-related ICs. In fact, we found that, on average, at least 30 PCs were required to explain more than 90% of the artifact variance, making the use of OBS (and consequently AAS) appropriate in the IC space, so as to preserve most of the physiological EEG variance contributing to the BCG-related ICs, while removing as much of the artifact variance as possible.

Several methods aiming at the selection of artefactual ICs from the decomposition of EEG data have already been proposed (Chaumon et al., 2015). Many of those, however, require prior knowledge regarding spatio-temporal characteristics underlying the EEG artifact that is to be removed, which is often translated into finding a single suitable template in both temporal and spatial domains (Abreu et al., 2015; Campos Viola et al., 2009; Wessel and Ullsperger, 2011). The

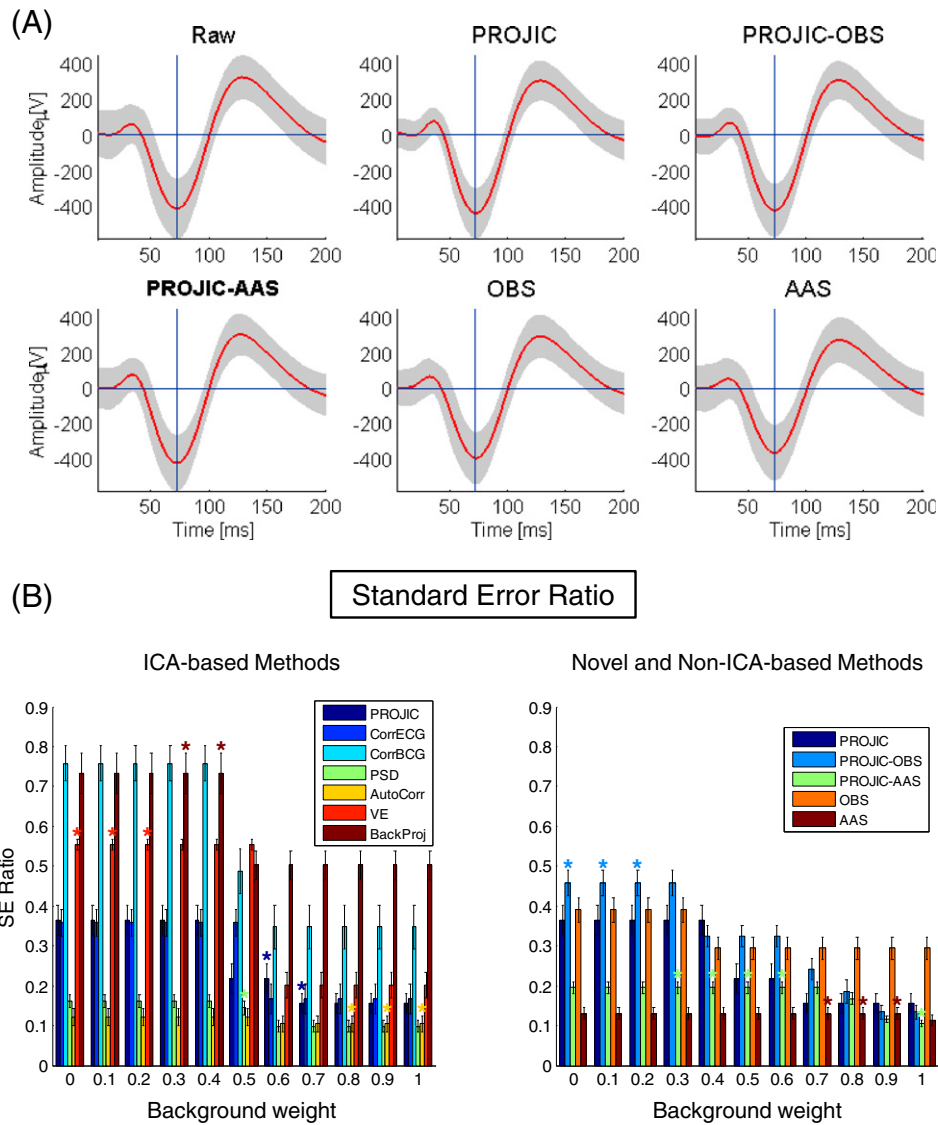


**Fig. 11.** IED quality improvement after BCG artifact correction, with optimized parameters for  $w_{bkg} = 0.5$ , for EEG recordings using Setup #1 at 3 T. (A) Representative average IED from P7 channel (in red), across trials. The gray area is defined by  $IED \pm 1STD$  (standard deviation). PROJIC, OBS and PROJIC-OBS exhibit a clear decrease in the inter-trial variability. PROJIC-AAS was the optimal method in terms of C for this background weight, highlighted in bold. (B)  $R_{SE}$  for each method and background weight, averaged across channels and subjects. The asterisks highlight the optimal method considering C. Only PROJIC-OBS, for  $w_{bkg} \leq 0.2$ , exhibited the best performance in terms of C and  $R_{SE}$  simultaneously.

non-stationary nature of the BCG artifact hinders the use of such methods, as no spatial template can be computed, thus narrowing the selection criteria to be temporal- or frequency-based exclusively.

#### Artifact removal vs. physiological signal preservation

Although BCG artifact correction is of the utmost importance in every simultaneous EEG-fMRI study (Mulert and Lemieux, 2009), the amount of artifact cleaning required in each case will strongly depend on the subsequent analyses that one wishes to perform on the corrected EEG data. In the time domain, the presence of the BCG artifact can tamper with the (manual or automatic) detection of events of interest, particularly IEDs, as their not-so-different morphology might mislead one into wrongly identifying them, possibly increasing the number of false positives (Kobayashi et al., 2001; Nayak et al., 2004; Siniatchkin et al., 2007). Additionally, it has been found that IED morphological features such as their amplitude, width or rising slope, may be correlated with the BOLD signal (Béнар et al., 2002; LeVan et al., 2010); the accurate extraction of such features would demand high performance of artifact correction algorithms, both in terms of artifact removal as well as

physiological signal preservation. In the frequency domain, spectral peaks related with the cardiac rate will always be present, which lie within frequency bands of interest for several EEG-fMRI studies, thus hampering the use of spectral EEG metrics as predictors of the BOLD signal (e.g., De Munck et al., 2009; Leite et al., 2013; Rosa et al., 2010). The study of trial-by-trial variations in ERPs is also in general highly dependent on an accurate artifact removal (e.g., Jorge et al., 2015a). In contrast to these situations, for a more conventional analysis of EEG-fMRI data of epileptic activity where IEDs are simply treated as all-or-none events, a moderate-quality artifact cleaning will probably be sufficient. In general, if one has no particular clues regarding the amount of artifact removal required, then the background weight and associated optimized method can be chosen as the ones yielding the highest combined ratio C.

#### Parameter optimization

An optimization on the subject level was first performed, motivated by the well-known high variability of the BCG artifact across time, channels and subjects. However, a relatively modest variability in the

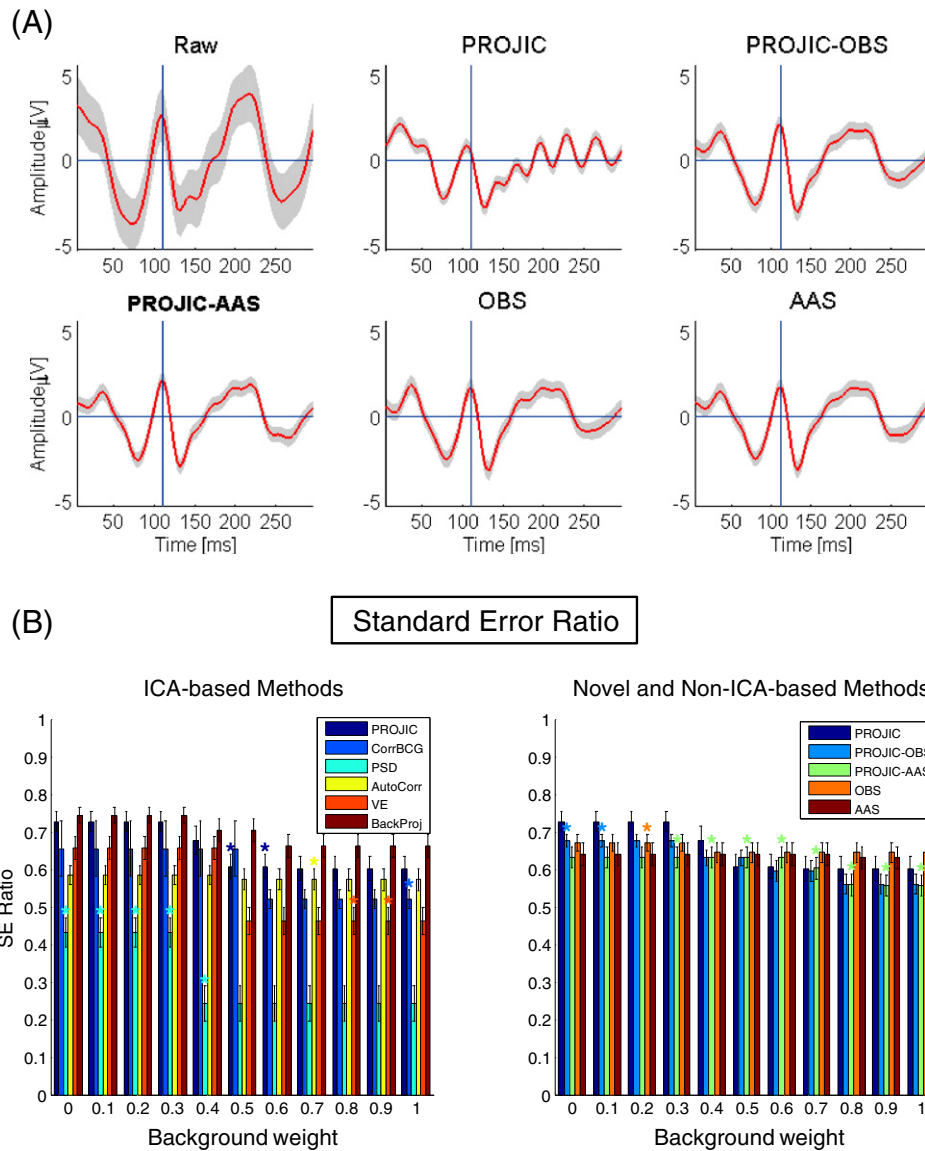


**Fig. 12.** VEP quality improvement after BCG artifact correction, with optimized parameters for  $w_{bkg} = 0.5$ , for EEG recordings using Setup #2 at 7 T. (A) Representative average VEP from POz channel (in red), across trials. The gray area is defined by  $VEP \pm 1SE$  (standard error). All methods exhibit a clear decrease in the inter-trial variability, and recovering the main features of the visual stimulation response. PROJIC-AAS was the optimal method in terms of C for this background weight, highlighted in bold. The PROJIC algorithm seems to introduce unexpected higher-frequency oscillations after the P100 component. (B)  $R_{SE}$  for each method and background weight, averaged across channels and subjects. The asterisks highlight the optimal method considering C. Comparable results across methods and background weights can be observed, although inconsistent with the optimal methods provided by the ratio C.

optimal parameter values of each algorithm was found across subjects, which was reflected in the statistically non-significant differences found between the performance obtained with subject- relative to group-level optimization. The latter allowed for the choice of the optimal method and associated set of parameters, for a given background weight, to be applied to all artifact-contaminated EEG datasets for each setup. Nevertheless, substantial variability was found regarding the optimal parameters across background weights, together with statistically significant effects of the optimization procedure on the performance of most methods. These results encourage the employment of the optimization step, despite the additional computational time it requires. This is in agreement with previous reports indicating that the use of default parameter settings for the more conventional artifact correction methods might not yield reasonable results, particularly at high magnetic field strengths (Debener et al., 2008). The optimization could also be performed on a channel-by-channel basis since typically high variability across channels and subjects was observed in terms of the BCG artifact occurrences, as well as in the spectral content of each

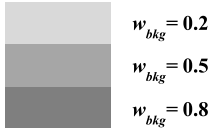
channel. This high variability, however, was taken into account by searching for the cardiac harmonics where a peak was observed, and then fine-tuning the spectral peak, more accurately quantifying the power within the artifact-related frequency windows and better informing the subsequent optimization procedure.

The use of different ICA algorithms with different parameters (for instance, the number of ICs to be estimated) would yield different EEG decompositions, which might interfere with the ultimate conclusions regarding the combination of optimal parameter settings and algorithm to correct EEG data for the BCG artifact, for a given background weight. As discussed in (Vanderperren et al., 2010), OBS and ICA only yielded comparable results whenever fine-tuning of the ICA parameters was performed, although no significant differences across different ICA algorithm implementations were found. These findings further support the hypothesis that the tuning of the parameter settings of the correction algorithms is of utmost importance (Debener et al., 2008).

Recently, real-time EEG-fMRI studies where human brain activity is non-invasively modulated resorting to neurofeedback mechanisms

**Table 1**  
Results of the post-hoc statistical testing for the performance of each correction method, on data collected using Setup #1 at 3 T. The red squares denote two correction methods that were not significantly different, in opposition with the blue squares (for instance, the PROJIC-OBS and PROJIC-AAS methods did not yield statistically significant differences in terms of the combined ratio C). A color-coded illustration of the combined ratio C of each correction method is shown in the diagonal for  $w_{bkg} = 0.2, 0.5, 0.8$ , also highlighting the methods exhibiting the best performance for a given background weight.

	PROJIC	PROJIC-OBS	PROJIC-AAS	OBS	AAS	CorrECG	CorrBCG	PSD	AutoCorr	VE	BackProj
PROJIC	0.55										
	0.60										
	0.73										
PROJIC-OBS		0.62									
		0.65									
		0.77									
PROJIC-AAS			0.59								
			0.69								
			0.78								
OBS				0.61							
				0.65							
				0.72							
AAS					0.55						
					0.67						
					0.79						
CorrECG						0.36					
						0.52					
						0.72					
CorrBCG							0.46				
							0.50				
							0.61				
PSD								0.53			
								0.60			
								0.70			
AutoCorr									0.37		
									0.54		
									0.73		
VE										0.61	
										0.55	
										0.67	
BackProj											0.60
											0.58
											0.61



$w_{bkg} = 0.2$   
 $w_{bkg} = 0.5$   
 $w_{bkg} = 0.8$

have been reported (Zich et al., 2015; Zotev et al., 2014). For our proposed methods to be appropriate for this purpose, a similar strategy to that described in (Becker et al., 2011) would need to be applied. First, a set of optimized parameters would be obtained either from another subject group studied with comparable acquisition setups, or from the same subjects in a previous acquisition. Second, a calibration run would be performed for each subject, in which ICA would be applied to the EEG data to obtain the un-mixing matrix, followed by the selection of BCG-related ICs using PROJIC, for instance. Thus, the time-consuming and computationally heavy procedures of both ICA decomposition and parameter optimization would be overcome. During the real-time EEG-fMRI acquisitions, Eq. (1) could be applied to the already acquired EEG, and the previously selected BCG-related ICs corrected for the artifact resorting to AAS or OBS, by exclusively using past artifact occurrences to build the artifact template that will be then subtracted from the data. However, if substantial differences on head movement are found between the calibration run and the real-time EEG-fMRI acquisitions, the use of the un-mixing matrix from the former as a spatial filter for the latter might not be applicable.

#### Evaluation pipeline

The novel evaluation pipeline we propose is designed for simultaneous EEG-fMRI data, and it relies on quantifying the physiological signal degradation within frequency windows neighboring those of the BCG artifact. A similar approach was proposed by (Freyer et al., 2009) for the quantification of the performance of gradient artifact correction methods. However, in this case, MR-silent periods were obtained by

means of an optimized EPI sequence (Anami et al., 2003) in which a long TR (4070 ms) was used, allowing for the acquisition of artifact-free EEG data in between the gradient artifact peaks at a cost of longer acquisition times. This method allows for a more accurate weighting between artifact and physiological signal removal than in our case, since EEG features such as the average spectral power, for instance, are computed within the same frequency windows for both conditions (scan and non-scan periods). Three ratios are defined to account for gradient artifact reduction, physiological signal removal and a combination of both, by comparing EEG features extracted from scan and non-scan periods, before and after each gradient artifact correction.

Although motivated by the more challenging task of assessing the performance of BCG artifact correction methods in resting-state data, our proposed evaluation pipeline could also be employed whenever events of interest are recorded on EEG. In particular, while some of the Setup #1 EEG captured IEDs, Setup #2 EEG registered VEPs. The optimal method for a given background weight, obtained based on our evaluation pipeline, was not always in agreement with the one yielding the greatest inter-trial variability reduction. Interestingly, the PROJIC-OBS and OBS methods yielded the highest standard error ratios for several background weights, particularly at 3 T. This is somewhat expected, since OBS is quite efficient at removing the BCG artifact by compromising the background physiological preservation. Thus, the inherent, and possibly of physiological relevance, variability of the ERPs might be unwantingly removed, which also raises the question of whether the standard error ratio is the most suitable performance metric. Nevertheless, it has been used previously for this purpose, which justifies its use in this study for comparison with previous reports (Niazy et al., 2005;

**Table 2**

Results of the post-hoc statistical testing for the performance of each correction method, on data collected using Setup #2 at 7 T. The red squares denote two correction methods that were not significantly different, in opposition with the blue squares (for instance, the PROJIC-OBS and AAS methods did not yield statistically significant differences in terms of combined ratio C). A color-coded illustration of the combined ratio C of each correction method is shown in the diagonal for  $w_{bkg} = 0.2, 0.5, 0.8$ , also highlighting the methods exhibiting the best performance for a given background weight.

	PROJIC	PROJIC-OBS	PROJIC-AAS	OBS	AAS	CorrBCG	PSD	AutoCorr	VE	BackProj
PROJIC	0.69 0.61 0.59									
PROJIC-OBS		0.72 0.67 0.68								
PROJIC-AAS			0.72 0.70 0.69							
OBS				0.73 0.67 0.63						
AAS					0.71 0.69 0.67					
Corr BCG						0.55 0.52 0.58				
PSD							0.71 0.60 0.52			
AutoCorr								0.60 0.60 0.60		
VE									0.64 0.58 0.60	
BackProj										0.67 0.60 0.59

$w_{bkg} = 0.2$   
 $w_{bkg} = 0.5$   
 $w_{bkg} = 0.8$

Vanderperren et al., 2010). Other performance metrics could also be used, such as: peak-to-peak values (Debener et al., 2008), ERP differences (Mantini et al., 2007), the SNR (Debener et al., 2007), trial-to-trial characteristics (Novitskiy et al., 2011) or the root mean square (RMS) (Freyer et al., 2009).

An evaluation pipeline taking into account both artifact and background ratios and one of the performance metrics described above could be desirable, better informing the subsequent optimization procedure of the BCG artifact correction algorithms, and also allowing for a more comprehensive assessment of the trade-offs between the artifact and physiological signal removal. However, similar SE ratios were found for the data used here, across methods and background weights, particularly at 7 T, possibly reflecting that this performance metric is not as discriminative of the method performances as the combined ratio C, and thus little would be gain by introducing it as a driving element of the optimization procedure.

As a rejection criterion from the artifact removal quantification for cardiac harmonics not exhibiting spectral peaks, thresholds based on the value of the convolution peaks between a Lorentzian function and cardiac-related power spectrum windows were used. Since these convolution thresholds were empirically determined, they are intrinsically data-dependent. Due to the relatively large number of EEG datasets tested in our study, particularly at 3 T, one can use the same convolution thresholds as a starting point in other studies; these thresholds, however, might need to be fine-tuned, in order to guarantee that the quantification of both artifact and background removal is as accurate as possible. Nevertheless, if comparable acquisition setups to those utilized in this study are used, the proposed thresholds could then be readily applied.

### Comparison between 3 T and 7 T setups

As expected from theory and previous results (Debener et al., 2008; Neuner et al., 2013), the BCG artifacts showed larger amplitudes in the 7 T setup when compared to those from 3 T. Small deviations from the theoretical linear relation between the BCG artifact amplitude and field strength observed are unsurprising given the considerable differences in the populations of each study. An important remark on this is that, although the amplitude of the BCG was much higher at 7 T, its relative variability seemed to be smaller to that at 3 T. This translates into larger artifact correction ratios for the 7 T when keeping the background weight constant. This line of results suggests that an important part of the variability of the BCG artifact is not intrinsic to the variability of the phenomena; if so, it should increase in the same proportion as the amplitude. Rather, that variability is possibly associated to other sources such as the ongoing EEG, for example.

Nonetheless, our results do now allow definite conclusions regarding the 3 T vs. 7 T comparison. In fact, our study is not particularly aimed nor designed to quantify the differences of the BCG artifact at different field strengths, as the population characteristics were not controlled for; further experiments would have to be performed to confirm these findings. Our goal is instead to illustrate the ability of the methods showcased here to handle very different acquisition scenarios, and crucially, to illustrate the importance of the optimization of the parameters in nearly all of the correction methods. It also aims to assess the consistency of the results and how generalizable the findings and recommendations are across different acquisition setups.

## Conclusion

We have proposed a novel method for the selection of BCG-related ICs, with three associated approaches for the correction of the BCG artifact in simultaneous EEG–fMRI, and have shown that they outperform both ICA-based and non-ICA-based state-of-the-art methods for most physiological background preservation weights. The PROJIC-OBS method returns the strongest attenuation of the BCG artifact, while the PROJIC-AAS method manages to preserve most of the physiological signal in the background with a small compromise of the artifact correction. For intermediate trade-offs, the AAS algorithm exhibits comparable results to PROJIC-AAS, the latter performing better in a wider range of background weights. Regardless of the desired level of physiological signal preservation, optimization of the algorithm's parameters is of the utmost importance. Clear data quality improvements on ERPs of interest were also observed, particularly at 7 T, where the subtle VEP features could be recovered after artifact correction. Overall, the consistency of the results across simultaneous EEG–fMRI data acquired with two different setups, a standard one at 3 T and a custom one at 7 T, indicates that these findings and recommendations may be generalizable across a wide range of EEG–fMRI acquisition setups.

## Acknowledgments

We acknowledge the Portuguese Science Foundation (FCT) for financial support through Project PTDC/SAUENB/112294/2009, Project PTDC/EEI/ELC/3246/2012, Grant UID/EEA/50009/2013 and the Doctoral Grant PD/BD/105777/2014. We also acknowledge Centre d'Imagerie BioMédicale (CIBM) of the UNIL, UNIGE, HUG, CHUV, EPFL and the Leenaards and Jeantet Foundations for providing the data acquired at 7 T.

## References

- Abreu, R., Leite, M., Leal, A., Figueiredo, P., 2015. STTICS: A template-based algorithm for the objective selection of epilepsy-related EEG ICA components. 2015 IEEE 12th International Symposium on Biomedical Imaging (ISBI). IEEE, pp. 343–346 <http://dx.doi.org/10.1109/ISBI.2015.7163883>.
- Allen, P.J., Josephs, O., Turner, R., 2000. A method for removing imaging artefact from continuous EEG recorded during functional MRI. *NeuroImage* 12, 230–239. <http://dx.doi.org/10.1006/nimg.2000.0599>.
- Allen, P.J., Polizzi, G., Krakow, K., Fish, D.R., Lemieux, L., 1998. Identification of EEG events in the MR scanner: the problem of pulse artefact and a method for its subtraction. *NeuroImage* 8, 229–239. <http://dx.doi.org/10.1006/nimg.1998.0361>.
- Anami, K., Mori, T., Tanaka, F., Kawagoe, Y., Okamoto, J., Yaritha, M., Ohnishi, T., Yumoto, M., Matsuda, H., Saitoh, O., 2003. Stepping stone sampling for retrieving artefact-free electroencephalogram during functional magnetic resonance imaging. *NeuroImage* 19, 281–295. [http://dx.doi.org/10.1016/S1053-8119\(03\)00048-X](http://dx.doi.org/10.1016/S1053-8119(03)00048-X).
- Becker, R., Reinacher, M., Freyer, F., Villringer, A., Ritter, P., 2011. How ongoing neuronal oscillations account for evoked fMRI variability. *J. Neurosci.* 31, 11016–11027. <http://dx.doi.org/10.1523/JNEUROSCI.0210-11.2011>.
- Bell, A.J., Sejnowski, T.J., 1995. An information-maximization approach to blind separation and blind deconvolution. *Neural Comput.* 7, 1129–1159. <http://dx.doi.org/10.1162/neco.1995.7.6.1129>.
- Bénar, C.-G., Aghakhani, Y., Wang, Y., Izenberg, A., Al-Asmi, A., Dubeau, F., Gotman, J., 2003. Quality of EEG in simultaneous EEG–fMRI for epilepsy. *Clin. Neurophysiol.* 114, 569–580. [http://dx.doi.org/10.1016/S1388-2457\(02\)00383-8](http://dx.doi.org/10.1016/S1388-2457(02)00383-8).
- Bénar, C.-G., Gross, D.W., Wang, Y., Petre, V., Pike, B., Dubeau, F., Gotman, J., 2002. The BOLD response to interictal epileptiform discharges. *NeuroImage* 17, 1182–1192. <http://dx.doi.org/10.1006/nimg.2002.1164>.
- Bonmassar, G., Purdon, P.L., Jääskeläinen, I.P., Chiappa, K., Solo, V., Brown, E.N., Belliveau, J.W., 2002. Motion and ballistocardiogram artefact removal for interleaved recording of EEG and EPs during MRI. *NeuroImage* 16, 1127–1141. <http://dx.doi.org/10.1006/nimg.2002.1125>.
- Campos Viola, F., Thorne, J., Edmonds, B., Schneider, T., Eichele, T., Debener, S., 2009. Semi-automatic identification of independent components representing EEG artefact. *Clin. Neurophysiol.* 120, 868–877. <http://dx.doi.org/10.1016/j.clinph.2009.01.015>.
- Chaumon, M., Bishop, D.V.M., Busch, N.A., 2015. A practical guide to the selection of independent components of the electroencephalogram for artefact correction. *J. Neurosci. Methods* <http://dx.doi.org/10.1016/j.jneumeth.2015.02.025>.
- Chowdhury, M.E.H., Mullinger, K.J., Glover, P., Bowtell, R., 2014. Reference layer artefact subtraction (RLAS): A novel method of minimizing EEG artefacts during simultaneous fMRI. *NeuroImage* 84, 307–319. <http://dx.doi.org/10.1016/j.neuroimage.2013.08.039>.
- De Munck, J.C., Gonçalves, S.I., Mammoliti, R., Heethaar, R.M., Lopes da Silva, F.H., 2009. Interactions between different EEG frequency bands and their effect on alpha–fMRI correlations. *NeuroImage* 47, 69–76. <http://dx.doi.org/10.1016/j.neuroimage.2009.04.029>.
- Debener, S., Mullinger, K.J., Niazy, R.K., Bowtell, R.W., 2008. Properties of the ballistocardiogram artefact as revealed by EEG recordings at 1.5, 3 and 7 T static magnetic field strength. *Int. J. Psychophysiol.* 67, 189–199. <http://dx.doi.org/10.1016/j.ijpsycho.2007.05.015>.
- Debener, S., Strobel, A., Sorger, B., Peters, J., Kranczioch, C., Engel, A.K., Goebel, R., 2007. Improved quality of auditory event-related potentials recorded simultaneously with 3-T fMRI: removal of the ballistocardiogram artefact. *NeuroImage* 34, 587–597. <http://dx.doi.org/10.1016/j.neuroimage.2006.09.031>.
- Debener, S., Ullsperger, M., Siegel, M., Fiehler, K., von Cramon, D.Y., Engel, A.K., 2005. Trial-by-trial coupling of concurrent electroencephalogram and functional magnetic resonance imaging identifies the dynamics of performance monitoring. *J. Neurosci.* 25, 11730–11737. <http://dx.doi.org/10.1523/JNEUROSCI.3286-05.2005>.
- Deburchgraeve, W., Cherian, P.J., De Vos, M., Swarte, R.M., Blok, J.H., Visser, G.H., Govaert, P., Van Huffel, S., 2008. Automated neonatal seizure detection mimicking a human observer reading EEG. *Clin. Neurophysiol.* 119, 2447–2454. <http://dx.doi.org/10.1016/j.clinph.2008.07.281>.
- Delorme, A., Makeig, S., 2004. EEGLAB: An open source toolbox for analysis of single-trial EEG dynamics including independent component analysis. *J. Neurosci. Methods* 134, 9–21. <http://dx.doi.org/10.1016/j.jneumeth.2003.10.009>.
- Freyer, F., Becker, R., Anami, K., Curio, G., Villringer, A., Ritter, P., 2009. Ultrahigh-frequency EEG during fMRI: pushing the limits of imaging-artefact correction. *NeuroImage* 48, 94–108. <http://dx.doi.org/10.1016/j.neuroimage.2009.06.022>.
- Grouiller, F., Vercueil, L., Krainik, A., Segebarth, C., Kahane, P., David, O., 2007. A comparative study of different artefact removal algorithms for EEG signals acquired during functional MRI. *NeuroImage* 38, 124–137. <http://dx.doi.org/10.1016/j.neuroimage.2007.07.025>.
- Iannotti, G.R., Pittau, F., Michel, C.M., Vulliemoz, S., Grouiller, F., 2014. Pulse artefact detection in simultaneous EEG–fMRI recording based on EEG Map topography. *Brain Topogr.* 28, 21–32. <http://dx.doi.org/10.1007/s10548-014-0409-z>.
- Jorge, J., Grouiller, F., Gruetter, R., van der Zwaag, W., Figueiredo, P., 2015a. Towards high-quality simultaneous EEG–fMRI at 7 T: detection and reduction of EEG artefacts due to head motion. *NeuroImage* 120, 143–153. <http://dx.doi.org/10.1016/j.neuroimage.2015.07.020>.
- Jorge, J., Grouiller, F., Ipek, Ö., Stoermer, R., Michel, C.M., Figueiredo, P., van der Zwaag, W., Gruetter, R., 2015b. Simultaneous EEG–fMRI at Ultra-high field: artefact prevention and safety assessment. *NeuroImage* 105, 132–144. <http://dx.doi.org/10.1016/j.neuroimage.2014.10.055>.
- Jorge, J., van der Zwaag, W., Figueiredo, P., 2013. EEG–fMRI integration for the study of human brain function. *NeuroImage* <http://dx.doi.org/10.1016/j.neuroimage.2013.05.114>.
- Kobayashi, K., Merlet, I., Gotman, J., 2001. Separation of spikes from background by independent component analysis with dipole modeling and comparison to intracranial recording. *Clin. Neurophysiol.* 112, 405–413. [http://dx.doi.org/10.1016/S1388-2457\(01\)00457-6](http://dx.doi.org/10.1016/S1388-2457(01)00457-6).
- Lee, T.-W., Girolami, M., Sejnowski, T.J., 1999. Independent component analysis using an extended infomax algorithm for mixed subgaussian and supergaussian sources. *Neural Comput.* 11, 417–441. <http://dx.doi.org/10.1162/0899766990300016719>.
- Leite, M., Leal, A., Figueiredo, P., 2013. Transfer function between EEG and BOLD signals of epileptic activity. *Front. Neurol.* 4 (JAN), 1–13. <http://dx.doi.org/10.3389/fneur.2013.00001>.
- LeVan, P., Tyvaert, L., Gotman, J., 2010. Modulation by EEG features of BOLD responses to interictal epileptiform discharges. *NeuroImage* 50, 15–26. <http://dx.doi.org/10.1016/j.neuroimage.2009.12.044>.
- Liu, Z., de Zwart, J.A., van Gelderen, P., Kuo, L.W., Duyn, J.H., 2012. Statistical feature extraction for artefact removal from concurrent fMRI–EEG recordings. *NeuroImage* 59, 2073–2087. <http://dx.doi.org/10.1016/j.neuroimage.2011.10.042>.
- Mantini, D., Perrucci, M.G., Cugini, S., Ferretti, A., Romani, G.L., Del Gratta, C., 2007. Complete artefact removal for EEG recorded during continuous fMRI using independent component analysis. *NeuroImage* 34, 598–607. <http://dx.doi.org/10.1016/j.neuroimage.2006.09.037>.
- Masterton, R.A.J., Abbott, D.F., Fleming, S.W., Jackson, G.D., 2007. Measurement and reduction of motion and ballistocardiogram artefacts from simultaneous EEG and fMRI recordings. *NeuroImage* 37, 202–211. <http://dx.doi.org/10.1016/j.neuroimage.2007.02.060>.
- Mijović, B., Vanderperren, K., Van Huffel, S., De Vos, M., 2012. Improving spatiotemporal characterization of cognitive processes with data-driven EEG–fMRI analysis. *Maced. Acad. Sci. Arts Sect. Biol. Med. Sci.* 33, 373–390.
- Mulert, C., Lemieux, L. (Eds.), 2009. *EEG–fMRI: Physiological Basis, Technique, and Applications*, first ed. Heidelberg, Dordrecht, London, New York, Springer Verlag.
- Mullinger, K.J., Havenhand, J., Bowtell, R., 2013. Identifying the sources of the pulse artefact in EEG recordings made inside an MR scanner. *NeuroImage* 71, 75–83. <http://dx.doi.org/10.1016/j.neuroimage.2012.12.070>.
- Murta, T., Leite, M., Carmichael, D.W., Figueiredo, P., Lemieux, L., 2015. Electrophysiological correlates of the BOLD signal for EEG-informed fMRI. *Hum. Brain Mapp.* 36, 391–414. <http://dx.doi.org/10.1002/hbm.22623>.
- Nayak, D., Valentín, A., Alarcón, G., García Seoane, J.J., Brunnhuber, F., Juler, J., Polkey, C.E., Binnie, C.D., 2004. Characteristics of scalp electrical fields associated with deep medial temporal epileptiform discharges. *Clin. Neurophysiol.* 115, 1423–1435. <http://dx.doi.org/10.1016/j.clinph.2004.01.009>.
- Neuner, I., Warbrick, T., Arrubla, J., Felder, J., Celik, A., Reske, M., Boers, F., Shah, N.J., 2013. EEG acquisition in Ultra-high static magnetic fields up to 9.4 T. *NeuroImage* 68, 214–220. <http://dx.doi.org/10.1016/j.neuroimage.2012.11.064>.

- Niazy, R.K., Beckmann, C.F., Iannetti, G.D., Brady, J.M., Smith, S.M., 2005. Removal of fMRI environment artefacts from EEG data using optimal basis sets. *NeuroImage* 28, 720–737. <http://dx.doi.org/10.1016/j.neuroimage.2005.06.067>.
- Novitskiy, N., Ramautar, J.R., Vanderperren, K., De Vos, M., Mennes, M., Mijovic, B., Vanrumste, B., Stiers, P., Van den Bergh, B., Lagae, L., Sunaert, S., Van Huffel, S., Wagemans, J., 2011. The BOLD correlates of the visual P1 and N1 in single-trial analysis of simultaneous EEG-fMRI recordings during a spatial detection task. *NeuroImage* 54, 824–835. <http://dx.doi.org/10.1016/j.neuroimage.2010.09.041>.
- Pan, J., Tompkins, W.J., 1985. A real-time QRS detection algorithm. *IEEE Trans. Biomed. Eng.* 32, 230–236. <http://dx.doi.org/10.1109/TBME.1985.325532>.
- Peng, H., Long, F., Ding, C., 2005. Feature selection based on mutual information: criteria of max-dependency, max-relevance, and min-redundancy. *IEEE Trans. Pattern Anal. Mach. Intell.* 27, 1226–1238. <http://dx.doi.org/10.1109/TPAMI.2005.159>.
- Rosa, M.J., Kilner, J., Blankenburg, F., Josephs, O., Penny, W., 2010. Estimating the transfer function from neuronal activity to BOLD using simultaneous EEG-fMRI. *NeuroImage* 49, 1496–1509. <http://dx.doi.org/10.1016/j.neuroimage.2009.09.011>.
- Rothlübbers, S., Relvas, V., Leal, A., Murta, T., Lemieux, L., Figueiredo, P., 2014. Characterisation and reduction of the EEG Artefact caused by the helium Cooling pump in the MR Environment: validation in epilepsy patient data. *Brain Topogr.* 28, 208–220. <http://dx.doi.org/10.1007/s10548-014-0408-0>.
- Salomon, R., Darulova, J., Narsude, M., van der Zwaag, W., 2014. Comparison of an 8-channel and a 32-channel coil for high-resolution fMRI at 7 T. *Brain Topogr.* 27, 209–212. <http://dx.doi.org/10.1007/s10548-013-0298-6>.
- Siniatchkin, M., Moeller, F., Jacobs, J., Stephani, U., Boor, R., Wolff, S., Jansen, O., Siebner, H., Scherg, M., 2007. Spatial filters and automated spike detection based on brain topographies improve sensitivity of EEG-fMRI studies in focal epilepsy. *NeuroImage* 37, 834–843. <http://dx.doi.org/10.1016/j.neuroimage.2007.05.049>.
- Srivastava, G., Crottaz-Herbette, S., Lau, K.M., Glover, G.H., Menon, V., 2005. ICA-based procedures for removing ballistocardiogram artefacts from EEG data acquired in the MRI scanner. *NeuroImage* 24, 50–60. <http://dx.doi.org/10.1016/j.neuroimage.2004.09.041>.
- Tenforde, T.S., Gaffey, C.T., Moyer, B.R., Budinger, T.F., 1983. Cardiovascular alterations in macaca monkeys exposed to stationary magnetic fields: experimental observations and theoretical analysis. *Bioelectromagnetics* 4, 1–9. <http://dx.doi.org/10.1002/bem.2250040102>.
- Tong, S., Bezerianos, A., Paul, J., Zhu, Y., Thakor, N., 2001. Removal of ECG interference from the EEG recordings in small animals using independent component analysis. *J. Neurosci. Methods* 108, 11–17. [http://dx.doi.org/10.1016/S0165-0270\(01\)00366-1](http://dx.doi.org/10.1016/S0165-0270(01)00366-1).
- Vanderperren, K., De Vos, M., Ramautar, J.R., Novitskiy, N., Mennes, M., Assecondi, S., Vanrumste, B., Stiers, P., Van den Bergh, B.R.H., Wagemans, J., Lagae, L., Sunaert, S., Van Huffel, S., 2010. Removal of BCG artefacts from EEG recordings inside the MR scanner: A comparison of methodological and validation-related aspects. *NeuroImage* 50, 920–934. <http://dx.doi.org/10.1016/j.neuroimage.2010.01.010>.
- Vanderperren, K., Ramautar, J., Novitski, N., Vos, M. De, 2007. Ballistocardiogram artefacts in simultaneous EEG- fMRI acquisitions. *Int. J. Bioelectromagn.* 9, 146–150.
- Wessel, J.R., Ullsperger, M., 2011. Selection of independent components representing event-related brain potentials: A data-driven approach for greater objectivity. *NeuroImage* 54, 2105–2115. <http://dx.doi.org/10.1016/j.neuroimage.2010.10.033>.
- Xia, H., Ruan, D., Cohen, M.S., 2014. Removing ballistocardiogram (BCG) artefact from full-scalp EEG acquired inside the MR scanner with orthogonal Matching pursuit (OMP). *Front. Neurosci.* 8, 1–12. <http://dx.doi.org/10.3389/fnins.2014.00218>.
- Yan, W.X., Mullinger, K.J., Geirsdottir, G.B., Bowtell, R., 2010. Physical modeling of pulse artefact sources in simultaneous EEG/fMRI. *Hum. Brain Mapp.* 31, 604–620. <http://dx.doi.org/10.1002/hbm.20891>.
- Zich, C., Debener, S., Kranczioch, C., Bleichner, M.G., Gutberlet, I., De Vos, M., 2015. Real-time EEG feedback during simultaneous EEG-fMRI identifies the cortical signature of motor imagery. *NeuroImage* 114, 438–447. <http://dx.doi.org/10.1016/j.neuroimage.2015.04.020>.
- Zotev, V., Phillips, R., Yuan, H., Misaki, M., Bodurka, J., 2014. Self-regulation of human brain activity using simultaneous real-time fMRI and EEG neurofeedback. *NeuroImage* 85 (Pt 3), 985–995. <http://dx.doi.org/10.1016/j.neuroimage.2013.04.126>.